Sérgio Miguel Rodrigues Fernandes

Bachelor of Science in Chemical and Biochemical Engineering

Spatially Controlled Surface Deposition of a Versatile ATRP Macroinitiator by Inkjet Printing

Dissertation to obtain the master's degree in Chemical and Biochemical Engineering

Advisor: Dr Joost Duvigneau, Visiting Assistant Professor, University of Twente.
Co-advisor: M. Sc.Marco Cirelli, PhD student, University of Twente.

Jury:

President: Prof. Mário Eusébio
Questioner(s): Dra. Teresa Casemiro
Vowel(s): Prof.ª Dra. Maria Miranda Reis

FACULDADE DE CIÊNCIAS E TECNOLOGIA
UNIVERSIDADE NOVA DE LISBOA

October of 2018

Blank page

Sérgio Miguel Rodrigues Fernandes

Bachelor of Science in Chemical and Biochemical Engineering

Spatially Controlled Surface Deposition of a Versatile ATRP Macroinitiator by Inkjet Printing

Dissertation to obtain the master's degree in Chemical and Biochemical Engineering

Advisor: Dr Joost Duvigneau, Visiting Assistant Professor, University of Twente.
Co-advisor: M. Sc.Marco Cirelli, PhD student, University of Twente.

Jury:

President: Prof. Mário Eusébio
Questioner(s): Dra. Teresa Casemiro
Vowel(s): Prof.ª Dra. Maria Miranda Reis

October of 2018

Blank page

Copyright

Spatially Controlled Surface Deposition of a Versatile ATRP Macroinitiator by Inkjet Printing

Blank page

Acknowledgements

First and for most, I would like to thank the MTP group for allowing me to do the dissertation within the group, in particular, G. Julius Vancso who is a person that I hold the utmost respect and admiration and also Joost Duvigneau that reminded me of a strong-willed that has clear purposes in mind as all good supervisors should have. Being my daily supervisor, I would like to thank Marco Cirelli, which inspired me with his long and intense working habits without never holding his smile throughout the day. I will always remember the traditional 10h30pm meetings and the memorable expressions such as “I will be right back, 30s” or the “tché” everytime I needed further explanation but more importantly, the “work hard, play hard” motto that sums pretty well the work hard but enjoy life personality that you have. I also wanted to thank everyone that was part of the MTP family during my time there for all the support and for the way you made me feel like a true member of the family. Particularly, I want to thank Clemens for all the help that he gave me and for showing me how I will be in the future, and Paola, my Erasmus “mom”, that was always there for me from day one to my final day. I won't forget the songs that we sang, our dinners, the late nights at the lab, the pool games or even the day I broke my and you went to buy one super early in the morning.

I want to thank my parents for always being there for me all these years and for allowing me to fulfil every experience that I craved to do during my university journey. I'm grateful that you were the rock I needed to hold to now fly for other experiences. To the rest of my family, thank you as well for accompanying me in this journey, and for all the words of encouragement when I was abroad.

Thank you as well to the many friends that I made throughout my journey as a university student and that without them this path would have lost its heart and its essence. Of those many friends, Kets and Catarina deserve a special mention for visiting me during my time in Twente and Gonçalo for the frequent conversations that we had as we both participated in the Erasmus program.

Last but not least, to all my friends outside the university and my friends from Nave de Haver that were with me all these years and that supported me in this final chapter of this last five amazing years. From family and friends that I made in the pass to the new connections that I made in the present, I’m truly happy to be surrounded by people that always wanted the best for me.

Blank page

Resumo

Funcionalização de superfícies de ouro para possíveis aplicações em revestimentos com uma técnica de deposição bem definida de um passo, nomeadamente, impressora de jato de tinta, foi alcançado de acordo com a seguinte metodologia:

Primeiramente, o macroiniciador de polimerização radical de transferência de átomos, *i.e* poli[metacrilato de 2-(2-bromoisobutiriloxy) etilo] (PBIEM) foi sintetizado através de transferência de fragmentação de adição reversível (RAFT) do metacrilato de 2-hidroxietil (HEMA) e a sua subsequente funcionalização com brometo de α-bromoisobutirilo (BIBB), ver esquema 5-1 e esquema 5-2. Espectroscopia de infravermelho por transformada de Fourier com reflectancia total atenuada (ATR FT-IR) e espectroscopia de ressonância magnética nuclear de protões (^{1}H-NMR) confirmaram a sucesso síntese de poli(HEMA), PHEMA, por RAFT, ver figura 5-2. A partir de ^{1}H-NMR, o peso molecular por número (M_n) de um precursor preparado foi determinado como sendo aproximadamente 23 kDa (6^{th} PHEMA). Esta funcionalização de PHEMA com BIBB foi também confirmado por ATR FT-IR e ^{1}H-NMR, ver figura 5-4 e figura 5-5.

Segundo, o PBIEM preparado foi depositado numa superfície de ouro através de impressão de jato de tinta. Diversas tintas foram produzidas sendo que a PBIEM-B (derivada da 6^{th} PHEMA) 10% (p/p) em N, N-dimetilformamida (DMF) rendeu camadas de enxerto mais densas. Medições de angulo de contacto de água (CA) e microscopia de infravermelho foram usadas para provar o enxerto do macroiniciador de ATRP em ouro. As imagens de altura do passo da microscopia de forca atómica (AFM) forneceram a espessura e rugosidade de camadas iniciadoras em superfícies de ouro. A espessura da camada de PBIEM obtida e de aproximadamente ~17 nm.

Por fim, as cadeias laterais constituídas por poli(N-isopropilacrilamida) (PNIPAM) foram sintetizadas via "grafting from" por ATRP para produzir estruturas do tipo escova de garrafa. Microscopia de infravermelho e AFM foram utilizadas para confirmar a fabricação bem-sucedida de polímeros escova de garrafa. Conversões ate 15% foram obtidos.

Palavras chave: Impressora de jato de tinta, polimerização RAFT, ATRP, escova de garrafa.

Blank Page

Abstract

Functionalization of gold surfaces for possible coating applications with a one-step pattern deposition technique in inkjet printing was achieved by the following methodology:

First, the atom transfer radical polymerization (ATRP) macroinitiator, *i.e.* poly[2-(2-bromoisobutyryloxy) ethyl methacrylate] (PBIEM) was synthesised by the reversible-addition fragmentation transfer (RAFT) polymerization of 2-hydroxyethyl methacrylate (HEMA) and its subsequent functionalization with α-bromoisobutyryl bromide (BIBB), see scheme 5-1 and 5-2. Attenuated total reflectance Fourier transform infrared spectroscopy (ATR FT-IR) and proton nuclear magnetic resonance spectroscopy (^{1}H-NMR) confirmed the successful synthesis of poly(HEMA) (PHEMA) by RAFT, see figure 5-2. From ^{1}H NMR spectra, the number-average molecular weight (M_n) of one prepared precursor was determined to be approximately 23 kDa (6th PHEMA). The functionalization of PHEMA with BIBB was confirmed by ATR FT-IR and ^{1}H-NMR spectroscopy as well, see figure 5-4 and figure 5-5.

Secondly, the prepared PBIEM was deposited on gold surface by inkjet printing. Several inks were produced being that the PBIEM (derived from 6th PHEMA 23kDa) 10% (w/w) solution in *N*, *N*-Dimethylformamide (DMF) yielded more dense grafting layers. Water contact angle measurements (CA), optical microscopy and infrared microscopy were used to prove the grafting of the ATRP-macroinitiator on gold. The atomic force microscopy (AFM) step height images provided the thickness and roughness and of deposit initiator layers on gold surfaces. The obtained PBIEM layer thickness is approximately ~17 nm.

Last, poly(*N*-isopropylacrylamide) (PNIPAM) side chains were synthesised *via* grafting from by ATRP to produce bottlebrush type structures. Infrared microscopy and AFM were used to confirm the successful fabrication of bottlebrush polymers. Conversions up to 15% were obtained.

Keywords: Inkjet printing, ATRP macroinitiator, RAFT polymerization, ATRP, bottlebrush.

Blank page

Table of Contents

Blank Page

Table of Figures

Blank Page

Table of Tables

Blank page

Table of Schemes

Blank page

Symbols and Abbreviations

μ	magnetic momentum
ν	vibration energy level
η	refractive index
Θ	angle
μCP	microcontact printing
^{1}H-NMR	Proton nuclear magnetic Resonance
AFM	atomic force microscopy
AIBN	2,2'-azobis-2-methylpropionitrile
ATR FT-IR	Attenuated total reflectance Fourier transform infrared spectroscopy
ATRP	atom transfer radical polymerization
^{n}BA	butyl acrylate
BIBB	α-bromoisobutyryl bromide
^{i}BnA	isobornyl acrylate
$CDCl_3$	chloroform-d
CPAD	4 cyano-4-(phenyl-carbonothioylthio) pentanoic acid
CRP	controlled radical polymerization
CTA	chain transfer agent
DEE	diethyl ether
DMF	*N*, *N*-Dimethylformamide
DMSO-d_6	dimethyl sulfoxide
DOD	drop-on-demand
DP_n	degree of polymerization
Fbg	Fibrinogen
FRP	free radical polymerization
HEMA	2-hydroxyethyl methacrylate
HEMA-TMS	2-(trimethylsilyloxy)ethyl methacrylate
M_n	molecular weight by number
MMA	methyl methacrylate
M_w	molecular weight by weight
NIPAM	*N*-isopropylacrylamide
NMP	nitroxide-mediated polymerization
OEGMA	oligo(ethylene glycol) methyl ether methacrylate

PBIEM	poly[2-(2-bromoisobutyryloxy) ethyl methacrylate]
PDEGA	poly[(di-ethylene glycol)ethyl ether acrylate]
PDI	polydispersity index
PGMA	poly(glycidyl methacrylate)
PHEMA	poly(2-hydroxyethyl methacrylate)
pLED	polymeric light-emitting diode
P(^{n}BA)	poly(*n*-butyl acrylate)
PMDETA	N,N,N',N'',N''-Pentamethyldiethylenetriamine
$PMEO_2MA$	poly(2-(2-methoxyehtoxy) ethyl methacrylate)
PMMA	poly(methyl methacrylate)
PRE	persistant radical effect
PS_t	poly(styrene)
RAFT	reversible-addition fragmentation transfer
THF	tetrahydrofruran
VA-044	2,2'-Azobis[2-(2-imidazolin-2-yl) propane] dihydrochloride

Chapter 1.

1.1 Introduction

Inkjet printing of polymer-based inks is an attractive non-contact patterning technique used for many applications due to its ability to precisely deposit small droplets of ink in well-defined patterns on various substrates providing enhanced surface properties, *e.g.*, multicolour polymeric light-emitting diode (pLED) displays and polymer electronics.(1, 2) In this project, we aim to functionalize gold surfaces with polymer brush patterns by *i*) grafting an ATRP macroinitiator with inkjet printing and *ii*) the subsequent growth of polymer brushes in the nanometre scale to be used in coating applications. Our approach will allow us to combine surface templating techniques and polymer brush synthesis to obtain surface properties on demand using a versatile fabrication technique to design patterned polymer brushes on the nanometre scale, bypassing the use of masters and stamps as in other common patterning techniques such as photolithography and microcontact printing (μCP).(3)

ATRP macroinitiators represent the future of coating technology as they enable the formation of complex architectural structures in bottlebrush type polymers films (molecules that are a subcategory of polymer brushes) that are very interesting since they may exhibit similar surface properties characteristic of polymer brush films, as said by Li et al. that reported the first study on surface properties of bottlebrush polymer thin films.(4) These films are currently used in the preparation of antifouling surfaces,(5-7) stimuli-responsive surfaces,(8, 9) By using bottlebrush polymers instead of brush polymers, higher grafting density surfaces can be achieved and also a higher efficiency towards a targeted application of choice due to specific homo or copolymer side chain configuration. Controlled radical polymerization techniques are critical in designing well-defined macromolecules as they provide control over molecular weight and dispersity. Of all these techniques, RAFT polymerization was chosen for the preparation of ATRP macroinitiators because is tolerant to most functional groups and contains a protected thiol,

typically dithioester, which is a direct pathway, to the assembly or immobilization of graft layers onto gold surfaces.(10)

For templating techniques, both photolithography(11) and μCP(12) (also known as soft lithography) have been used to pattern surfaces however, inkjet printing potential is immense even for areas that this technique has not been used before as described by Berend-Jan de Gans and Ulrich S. Schubert.(13) Inkjet printing is very attracting technique because it's completely digital thus changing the printing design has little further cost impact.(14) Other advantages of inkjet printing include tunability of the ink formulation, the overall flexibility of the technology, easy reproducibility (possibility of automatization) and the possibility of depositing very small amounts of material.(1)

1.2 Theoretical introduction

1.2.1 Controlled Radical Polymerization (CRP)

Due to its simplicity, free radical polymerization (FRP) has been widely adopted in many industrial and laboratory scale polymerization processes since its maturity in the 1950s and 1960s.(15) In the last four decades, however, research efforts have been shifted to unveil new techniques that allowed the production of macromolecules with controlled structures not achievable in FRP mechanisms. It was with the discovery of living anionic polymerization by Michael Szwarc in 1956 that made the pathway for major developments in other polymer synthetic areas that allow the production of well-defined polymers with precise molecular architectures.(16) The new techniques based on CRP, because of its inherent radical intermediaries they possess similar limitations as in FRP, namely chemo-, regio-, stereo-selectivities and unavoidable radical termination.(16) However, in contrast to FRP, where all chains terminate, only a fraction of active chains between 1 and 10% terminate in CRP. The remaining dormant chains are capable of reactivation, functionalization and chain extension to form other structures such as block copolymers.(17) As it's the case in designing complex structures to produce macromolecules with defined molecular weight and very narrow polydispersity it is critical that all chains grow simultaneously via nearly instantaneous initiation and that chain termination reactions are minimized. This concept derives from living polymerization that by definition is a chain growth process without chain breaking reactions such as transfer or termination.(18, 19) Polymerizations that combines fast initiation and an absence of termination reactions have the potential to obtain well defined macromolecular structures. So often this CRP is called living radical polymerization, however, it is important to note that due to

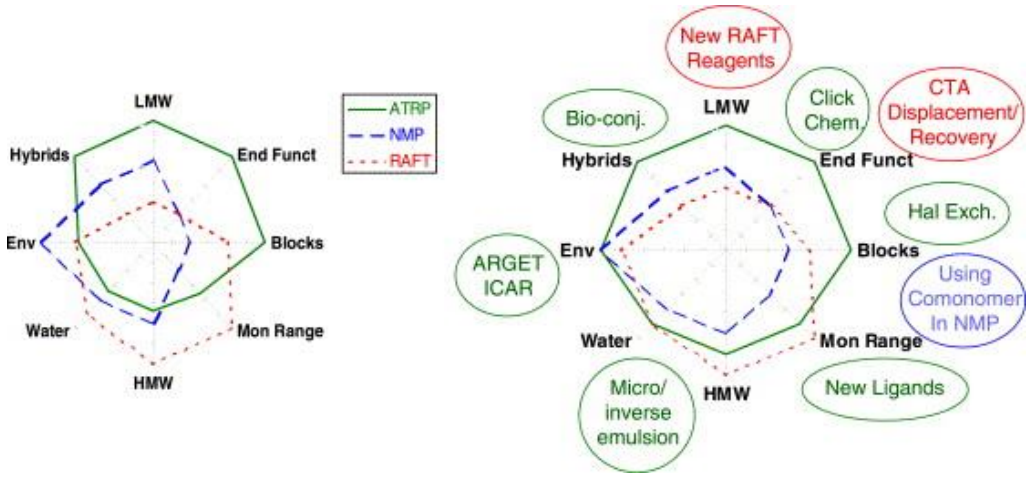

Figure 1-1 (16,33) Comparation between RAFT, ATRP and NMP in the areas related to the synthesis of low molecular weight (LMW), end functional polymers (End Funct), block copolymers (Blocks), range of polymerizable monomers (Mon Range), synthesis of various hybrid materials (Hybrids), environmental issues (Env) and polymerization in aqueous media (Water).

the inherent nature of radical reactions, particularly coupling or disproportion, it's impossible to have a polymerization reaction completely absence of termination reactions and so it is only possible to develop polymerization conditions that exhibit living characteristics.

There are three main mechanisms that have been used to achieve controlled radical polymerization. The first mechanism is the reversible recombination of growing radicals with scavenging radicals namely nitroxide-mediated polymerization (NMP) first described by Solomon and Rizzardo.(20) (21) The first example of this mechanism is the thermal polymerization of controlled styrene chains with a stable free radical TEMPO as described by Georges et al. in 1993.(22) Currently the scope of NMP has greatly expanded over the years with better control of a wide variety of monomers.(23) The second mechanism is the reversible termination of growing radicals as it is found in ATRP that are trapped in transition metal complexes. Metal such Li(24), Mo(25), Re(26), Fe(27, 28), Ru(29), Ni(30) and Cu(31) are proven to successfully mediate ATRP reactions.(16) The third mechanism is based on a degenerative exchanging process involving reversible chain transfer as in RAFT. High molecular conversions (≈95%) of methyl methacrylate and butyl methacrylate have been reported.(32) Comparison between this three techniques from a target structure is given (figure 1-1) where the left side indicates the state of the techniques in 2002 and the right side indicates the latest comparison in 2006, as described by Matyjaszewski.(16, 33) It is also important to notice that, in concordance with the major developments shown in figure 1-1 regarding the ATRP capacity to control macromolecular architecture, perhaps due to not only the inherent mechanisms characteristic of this technique but also the numerous derivations processes from ATRP that have been created that greatly expanded the current possible applications, the cumulative number of publications

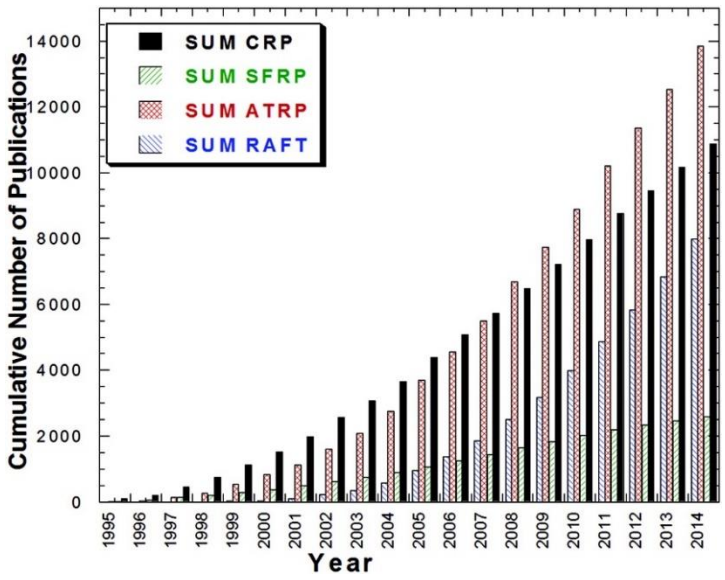

Figure 1-2 (17) Scifinder results on the legend topics.

regarding this technique also increased far over the other CRP techniques (figure 1-2) being the possible main reason the many commercially available reagents synthesised under undemanding reaction conditions.(34)

1.2.2 RAFT polymerization

RAFT polymerization, as a CRP technique, it has the ability to allow the fabrication of predetermined structures such as amphiphilic block copolymer chains, star polymers and other complex architectures, end functional polymers and self-assembly and/or stimuli-responsive polymers.(15) The most common mechanism for RAFT polymerization is shown in scheme 1.1. Initiation occurs as in conventional radical polymerization: for example, thermal decomposition of radical initiators is more widely used than other reported sources such as thermal autoinitiation of monomers, photochemical reaction of the chain transfer agent, CTA, by ultraviolet light, gamma radiation and pulsed laser irradiation(36). In step 1 of the initiation process, polymeric radicals are formed ($P_n^{\bullet}$) upon monomer addition to the initiator species. The propagating radicals produced in this step react with the chain transfer agent, CTA, (**1**) in step 2 of initialization. The radical intermediate (**2**) fragments reverting to its original composition or forms a polymeric structure named macro-RAFT agent (**3**) and a new radical ($R^{\bullet}$). The propagation step sees those radicals ($R^{\bullet}$) reacting with monomer units further growing the polymer chains ($P_m^{\bullet}$). The new propagation radical rapidly reaches a chain equilibrium between the active propagating radical and the dormant polymeric macro-RAFT agent complex.(37) The rapid degenerative exchange (k_{addP}) that originates the stabilized radical intermediate (**4**), ensures the equal probability for all chains to grow with roughly the same dispersity since rapid exchange sees the concentration of

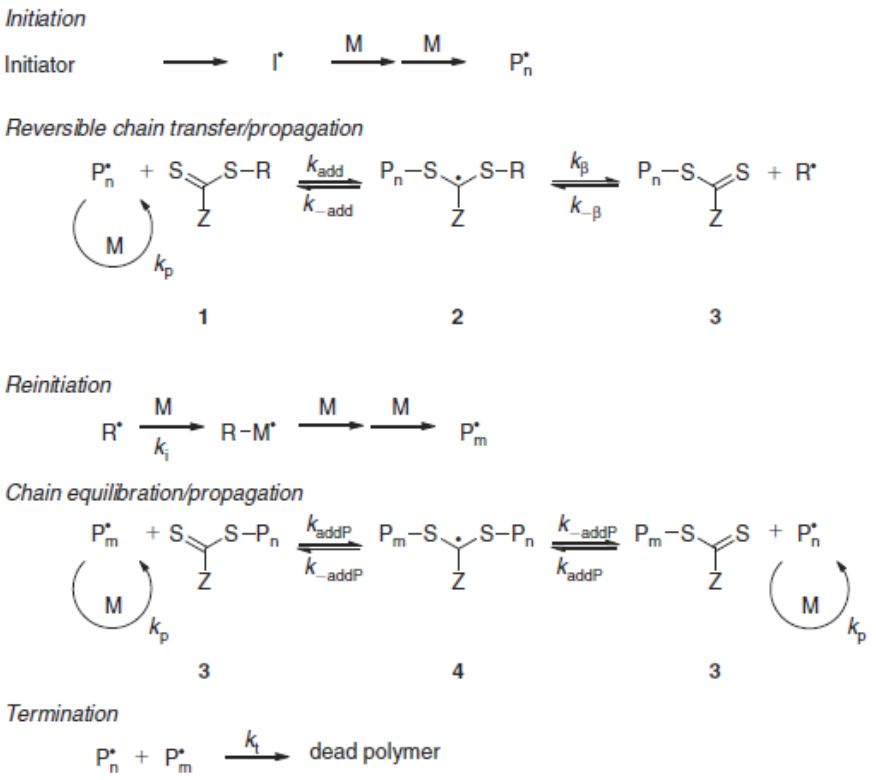

Scheme 1-1 (35) RAFT polymerization mechanism.

radicals be kept lower than (**4**) and thus limiting termination reactions.(36) Termination events, like the initiation step, also occur in concordance with FRP meaning this termination processes can occur *via* combination or disproportionation mechanism.(36)

Since systems that are ruled by degenerative transfer follow typical FRP kinetics to be able to obtain macromolecules with a narrow polydispersity index (PDI), the appropriate choice of CTA must carefully be made. The Z and R groups (**1**) play a critical part in this selection as the first one determines the reactivity towards propagating radical and the stability of the intermediate radicals (**2** or **4**, respectively) and the last one, being the homolytic leaving group, it determines the leaving group ability and the reinitiation efficiency of R• that should be $\geq k_p$.(37) Quantitatively speaking the properties of RAFT agents can be determined by two transfer coefficients, C_{tr} ($=k_{tr}/k_p$) and C_{-tr} ($=k_{-tr}/k_i$) where k_{tr} and k_{-tr} are the rate constants for chain transfer, k_p and k_i are the rate constant for propagation and initiation, respectfully. The linear dependence of molecular weight on conversion and low dispersity (PDI< 1.2) typical of living polymerizations require a C_{tr} of at least 10, however more effective RAFT agents have $C_{tr} > 100$.(38)

1.2.3 ATR polymerization

ATRP was reported for the first time independently in 1995 by Mitsuo Sawamoto,(39) Krzysztof Matyjaszewski and Jin-Shan Wang.(40) This mechanism relies on the persistent radical effect (PRE).(41, 42) The PRE is a kinetic feature which promotes a self-regulation effect in all CRP systems that obey this parameter. Propagating radicals (P_n^*) are trapped in a deactivation process (k_{deact}) with persistent radicals (Mt^{n+1}/L), scheme 1-2. Those radicals cannot terminate with each other, unlike the propagating radicals, but only cross-couple with the growing radicals. Thus, with time the concentration of radicals as well as the probability of termination reactions decrease due to the irreversible accumulation of persistent radicals caused by radical-radical termination and so growing radicals are predominantly reacting with chemical species.(16) The dormant species, which exists in the form of alkyl halides, for example, a macromolecular species (P_n-X), periodically reacts with an activator as in the transition metal complex (k_{act}) in their lower oxidation state, Mt^n/L (Mt^n represents the transition metal species with an oxidation state of n and L is the ligand), forming the growing radicals that can propagate with the vinyl monomer (k_p) and a deactivator in the form of a transition metal species with a higher oxidation state, as a result of halide connection, $X\text{-}Mt^{n+1}/L$.(34) The propagating radicals formed can also terminate as in FRP or be reversibly deactivated to the dormant chain state. To obtain polymeric chains with low polydispersity values is necessary to have high monomer conversions (p), high degree of polymerization by number (DP_n), a high concentration of the polymer chain in a dormant state (P_n-X) and small ratios of k_p/k_{deact} (equation 1-1). According to the equation 1-1, note that low concentrations of catalysts can be used and still provide control over the polydispersity if they have sufficiently high values of k_{deact}, however, the amount of transition metal cannot indefinitely decrease as it requires a sufficient concentration of deactivator.(16)

Equation 1-1 PDI equation for ATRP reactions.

$$\mathrm{PDI} = \frac{M_w}{M_n} = 1 + \frac{1}{DP_n} + \left(\frac{k_p[P_n - X]}{k_{deact}[X - Mt^{n+1}/L]}\right)\left(\frac{2}{p} - 1\right)$$

Moreover, the key for a successful reaction, the ATRP equilibrium ($K_{ATRP}=k_{act}/k_{deact}$) must be strongly favoured towards the dormant species meaning rate constant of deactivation must be substantially bigger than the rate constant of activation. Factors such the structure of the ligand, monomer/dormant species compatibility and reaction conditions (*e.g.* temperature, pressure, solvent) can significantly influence the values of the rate constants, k_{act} and k_{deact} and thus, k_{ATRP}.

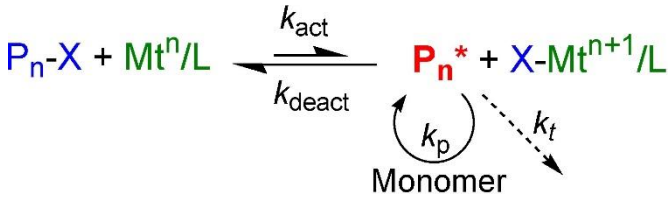

Scheme 1-2 (43) ATR polymerization overall mechanism.

1.2.4 Inkjet Printing

In order to functionalize surfaces, the appropriate deposition technique has to take into account the targeted final application. Solvent-based techniques, such as spin-coating, dip-coating and inkjet printing can be used to prepare bottlebrush thin film layers however this last type of modifying surfaces have not been reported until Li et al. study.(4) Inkjet printing is a complex technique capable to deposit a variety of inks with different properties and thus requires the appropriate care for successful printing deposition.

There are two modes to deposit polymers based inks: continuous or drop-on-demand (DOD) (Figure 1-3). In continuous mode, the ink is pumped through a nozzle forming a continuous stream of sized droplets. The generated droplets are selectively charged via signals from the printer by being subjected to an electrostatic field. The charged drops are then deflected in a deflection field, which determines where the drop lands.(44) Depending on the system used, the charged droplets can be printed onto the matrix or collected into a recirculation system to be later reused. Continuous mode can print at high speeds, the nozzle is not easily clogged and has the ability to use inks based on volatile solvents allowing rapid drying adhesion. Disadvantages to this mode include low print resolution, the use of inks that are capable of being charged, high investment cost as the printer has a drop selection section and a recycling unit followed by high maintenance costs.(45) On drop-on-demand mode, a pressure pulse is created to eject ink droplets

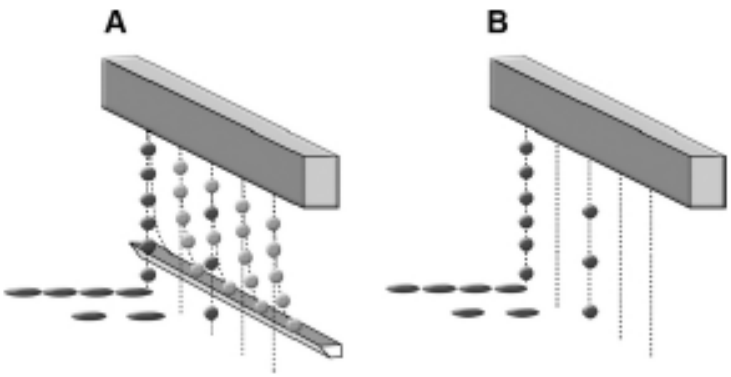

Figure 1-3 (44) Schematic representation of continuous (A) and drop-on-demand inkjet printing (B).

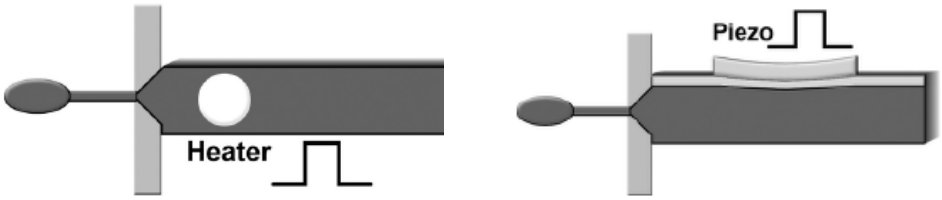

Figure 1-4 (44) Representation of DOD inkjet printing mechanisms: Thermal (left side) and piezoelectric (right side).

through a nozzle. DOD inkjet printers main deposition technologies are either thermally or piezoelectrically.(46) Thermal inkjet printers (Figure 1-4 left side) rely on rapidly heating up the ink present in the ink chamber, with the use of a resistor, to temperatures high enough to vaporize the ink. This instantly pushes the ink droplet out through the nozzle until all the heat stored in the ink is used, then the bubble collapses and refills the chamber.(47) Piezoelectric inkjet printers (figure 1-4 right side) materials deform when submitted to an electric impulse and it's through this mechanism that the ink is ejected out of the nozzle. Additionally, because this types of printers are not regulated by heating processes they accept a wider range of inks and they possess print heads that last longer in comparison with thermal print heads.(45)

There are currently four main types of inks used: phase-change, solvent-based, water-based and UV curable.(44) Within the direction of this work, the inks formulated insert themselves in the solvent-based inks, more precisely additives. A major factor for successful printing relies on the ink rheological properties, particularly the viscosity and the surface tension. The viscosity should be low, typically below 20 cP, as higher values have the potential danger of viscously dissipating too much kinetic energy preventing droplet ejection.(1) The spheroidal shape of the liquid drop is controlled by the surface tension and its behaviour can be theoretically predicted with a physical constant named Weber number, with fluids with high Weber values, are more likely to present non-spheroidal shapes. Considering all the factors for successful printing mentioned above, a commonly used parameter to indicate the capacity for good printability is the Z parameter [the inverse of the Ohnesorge number (Oh)], where values between 1 and 10 are expected to generate stable drop formation.(45)

Besides the rheology properties of the ink, to ensure define printability, ink formulation must also be compatible with wettability to ensure that the ink and the substrate reach a phase of equilibrium between themselves and the environment which is translated in the minimum Gibbs energy state that corresponds to the most stable state named apparent contact angle.(44)

Chapter 2. State of Art

2.1 ATRP Macroinitiator

ATRP macroinitiators are polymers that are functionalized with an initiating group along the polymer backbone(48) As their name suggests, these types of macromolecules are used in ATRP systems which is a subgroup of CRP techniques as described in subchapter 1.2.1. ATRP initiator and macroinitiators consist of alkyl halides structures and both are a critical part of ATRP reactions as they enable the formation of well-defined polymers. Examples of complex structures obtained with ATRP macroinitiators are represented below:

Matyjaszewski et al.(49) synthesized hybrid materials composed of inorganic poly(siloxanes) macroinitiators. ABA Triblock copolymers obtained from difunctional poly(dimethylsiloxane) with benzyl chloride and 2-bromoisobutyryloxy (BIBB) coupled initiators were used to polymerize a variety list of monomers, namely styrene, isobornyl acrylate and n-butyl acrylate (^{n}BA) for the first initiator and methyl methacrylate and 2-(trimethylsilyloxy)ethyl methacrylate (HEMA-TMS) for the second initiator. They discovered that with higher molecular weight macroinitiator significant decreases in polydispersities were observed.

Miura et al.(50) synthesised an AB_{20}-type heteroarm star polymer consisting of poly(styrene) (PS_t) arm and 20-arms of poly(methyl methacrylate) PMMA or poly(^{t}BA). The ATRP macroinitiator was obtained with the following steps: NMP of styrene using mono-6-[4-1'-(2",2",6",6"-tetramethyl-1"-piperidinyloxyethyl)benzamido]-b-cyclodextrinperacetate named as **1**) to have PS_t end-functionalized with the β-CyD unit, prepolymer as they call it (**2**); After deacetylation of the prepolymer, the ATRP macroinitiator is formed (**3**) and the complex structure prepared was obtained after reacting with 20 (2-bromoisobutyrol)s.

Cheng at al.(51) designed a norbornenyl-functional ATRP initiator by combining an exo-norbornenyl functionality and α-bromoisobutyrate with a $-CH_2O(CH_2)_{10}$ spacer. Novel

nanostructures were not synthesised and were in progress since the main focus of the article was the preparation of new α- norbornenyl macromonomers by ATRP.

Liu et al.(52) studied the relationship between the amount of initiator anchored to the surface and the rate of the brush layer grafted. An anchoring polymer layer consisted of poly(glycidyl methacrylate) (PGMA) was deposited by dip-coating in a silicon substrate and the attachment of the bromoacetic acid (BAA) was made to an unannealed as well as a preannealed PGMA layer, observing that preannealed film originated smooth and uniform surface morphology. PS_t brushes were synthesised and they concluded that the increase in the surface density of initiating moieties led to the increase in the grafting rate, however, a limit concentration where the increase of initiator layers had no effect on the grafted layer was observed.

More recently, Cabane et al.(53) attempting to bring new functionalities into wood they reported the synthesis of functional lignocellulosic materials with novel properties not have been reported before. (*Picea abies*) wood samples were coupled with BIBB yielding a solid ATRP macroinitiator denoted as W-Br. *In situ* polymerizations of styrene, NIPAM were performed within the bulk wood structure.

2.2 Bottlebrush polymer synthesis

Targeting more the last concept of this work, final application bottlebrush structures obtained with ATRP macroinitiators are given: Beers et al.(54) prepared brush copolymers of homopolymer side chains that consisted of PS_t and P(^{n}BA). Two different approaches were used to prepare ATRP macroinitiators for brush copolymer synthesis: In the first approach, FRP was utilized to polymerize 2-(2-bromopropionyloxy) ethyl acrylate using 2,2'-azobis-(2-methylpropionitrile) (AIBN); in the second approach trimethylsilyl protected HEMA-TMS was polymerized *via* ATRP and subsequently esterified with BIBB in the presence of a catalytic amount of tetrabutylammonium fluoride.

Janata et al.(48) fabricated multifunctional ATRP macroinitiators starting with low molecular weight PS_t and poly(4-methyl styrene). For the first macromolecule, three-step functionalization procedure was performed to synthesise the ATRP macroinitiator: Friedel-Craft acylation with acetyl chloride; reduction of carbonyls to secondary hydroxy with lithium aluminium hydride; esterification with 2-bromopropionyl bromide or BIBB. For the latter polymer, direct esterification using *N*-Bromosuccinimide as a brominating agent under AIBN and dry carbon tetrachloride conditions were used.

Neugebauer et al.(55) in attempted to understand the grafting density of brush molecules with different side chain lengths, they prepared a series of cylindrical brushes of PMMA and

poly(^{n}BA) *via* grafting from. These molecules were prepared with a multifunctional macroinitiator, PBIEM developed by ATRP of HEMA-TMS. By analysing the side chains detached using solvolysis, they observed with PMMA side chain using copper(I) chloride/copper(II) chloride/4,4′-Dinonyl-2,2′-dipyridyl catalyst system, a grafting efficiency cap at approximately 50%. They concluded that the low grafting density was due to the 2-bromoisobutyrate initiating moieties being non-ideal for the ATRP of methacrylates.

Venkatesh et al.(56) utilized the combination of RAFT and ATRP to synthesise polymer brushes using grafting from or a combination of grafting through and grafting from. PBIEM and poly[BIEM-co-poly(ethylene glycol) methyl ether methacrylate] grafted copolymers based ATRP macroinitiators were used to form brushes consisting of both homopolymer side chains of methyl methacrylate, and statistical copolymer side chains of MA and 1-octene.

Fleet et al.(57) reported the synthesis of novel glycopolymer brushes of 6-O-MMAGIc methyl methacryloyl-α-D-glucoside, using sequential RAFT-mediated polymerization of homopolymer PBIEM and copolymers P(BIEM-co-MMA), P(MMA-block-BIEM), poly(4-vinylbenzyl chloride-alt-maleic anhydride) backbones, followed by ATRP of these macroinitiators.

Mukumoto et al.(58) synthesised *via* grafting from molecular bottlebrushes with hydrophobic P(^{n}BA) and hydrophilic PSt and poly[di-(ethylene glycol) ethyl ether acrylate] (PDEGA) side chains. For this procedure, an iron-based ATRP method with iron(II) bromide /iron(III) bromide/ tetrabutylammonium bromide catalyst system was utilized using PBIEM as a macroinitiator. AFM characterization of bottlebrushes show a number-average contour length L_n between approximately 119 to 130 nm (Figure 2-1).

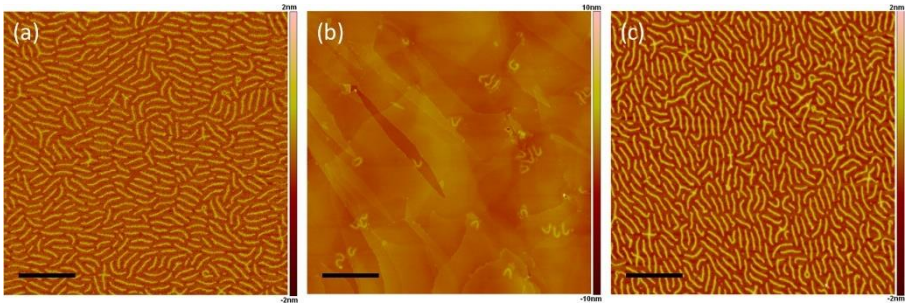

Figure 2-1 (58) AFM images of molecular bottlebrushes as presented in the article: (a) PBIEM-graft-P(^{n}BA), (b) PBIEM-graft-PS_t, and (c) PBIEM-graft-PDEGA. All scale bars have 400 nm length.

2.3 Exemplar though-out applications

A few possible final applications within advanced coating surfaces of designed bottlebrush structures originated from the inkjet printed ATRP macroinitiator is presented.

2.3.1 Antifouling surfaces

In order to tackle a significant challenge in biotechnology, Zamfir et al.(59) utilized S-RAFT polymerization of protein resistant HEMA brushes up to 70 nm. According to the literature searched by the authors, protein fouling challenges the precise control of the interactions at the interface of biomaterials as it leads to non-specific responses in affinity biosensors, can lead to bacterial attachment, immune response to biomaterials, among others. PHEMA brushes were submitted to two main plasma proteins, human serum albumin and fibrinogen (Fbg) and they showed excellent resistance to fouling, proving that a minimum of 20 nm brushes was needed to fully prevent the fouling.

Li et al.(60) prepared poly(oligo(ethylene glycol) methyl ether methacrylate-b-glycidyl methacrylate) (POEGMA-block-PGMA) di-block copolymer brushes on flat silicon wafers via consecutive SI-AGET ATRP. They not only reported bioactive surfaces that were resistant to proteins such as Fbg and lysozyme but also concluded that the conjugation of bioactive molecules could be controlled by varying the thickness of the brush layers produced.

2.3.2 Stimuli-responsive surfaces

Thermo-switchable bioactive surfaces relevance toward creating smart materials for controlling bio-adhesion is increasing very significantly.(61) With this in mind, nanopatterned brushes with tunable topography of a thermo-responsive polymer, poly(2-(2-methoxyehtoxy) ethyl methacrylate) ($PMEO_2MA$) was synthesised and its response to external stimulus in water at variable temperatures was studied by Jonas et al.(62)

A year before, the same author,(63) first reported the synthesis of the copolymer $PMEO_2MA$-co-OEGMA by surface-initiated ATRP that allowed switchable surface properties. These brushes, contrary to PNIPAM which shows moderate cytotoxic behaviour at 37^{o}C, are nontoxic and thus are more biocompatible for thermoresponsive surface applications located.

Chapter 3. Intruments Theory

3.1 NMR

NMR spectroscopy is one of the more widely used characterization techniques since it provides the most direct and general tool for identifying the structure of both pure compounds or mixtures organic or inorganic making this a very powerful technique.(64)

NMR key aspect is based on the concept of nuclei intrinsic angular momentum or spin. Since the spinning nuclei are positively charged, it generates a magnetic field, with it a magnetic momentum, μ.(64) The atomic mass (sum of the atom's protons and neutrons) governs the overall spin on the nucleus. When the atomic number (the number of protons in an atom) equals the atomic mass the nucleus has no magnetic properties and so the spin quantum number, *I*, equals zero (Figure 3-1). If the atomic number or the atomic mass is odd, or booth are odd, the nucleus has magnetic properties and shows spin quantum number that can only take certain numbers.

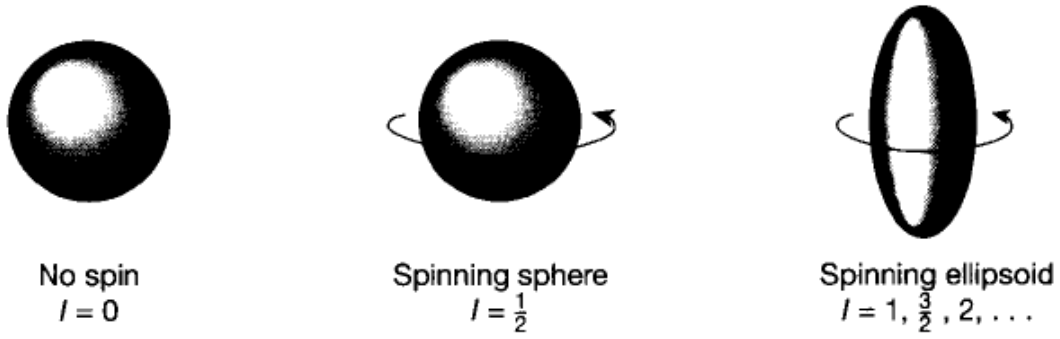

Figure 3-1 (64) Three classes of nuclei spin.

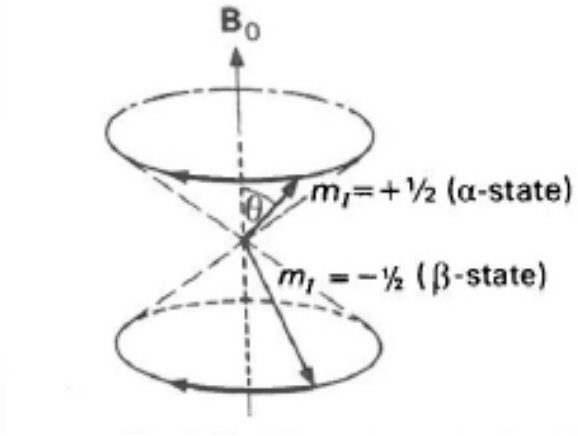

Figure 3-2 (65) Precessional range of motion for a spin $\frac{1}{2}$ nuclei under a magnetic field.

Nuclei, such as ^{1}H and ^{13}C, have a spin of $\frac{1}{2}$ because their nuclei have a spherical shape and nuclei with a nonspherical, or quadropolar shape, have a spin of 1 or more, with increments of half-integers of $\frac{1}{2}$.(64) In the absence of magnetic field, all nuclei of the same isotope have the same energy, however, when applied a magnetic field, B_o, there are $2I+1$ equally spaced spin states according to their values of I. For example nuclei with spin of $\frac{1}{2}$ assume only 2 arrangments ($+\frac{1}{2}$ of slight less energy then $-\frac{1}{2}$) (Figure 3-2) being that the separation of spin states is called the Zeeman effect.(66)

NMR experiment (Figure 3-3), more precisely ^{1}H-NMR, consists in applying a strong magnetic field, B_o, in order to the distinguish the nuclei spin states followed by the application of

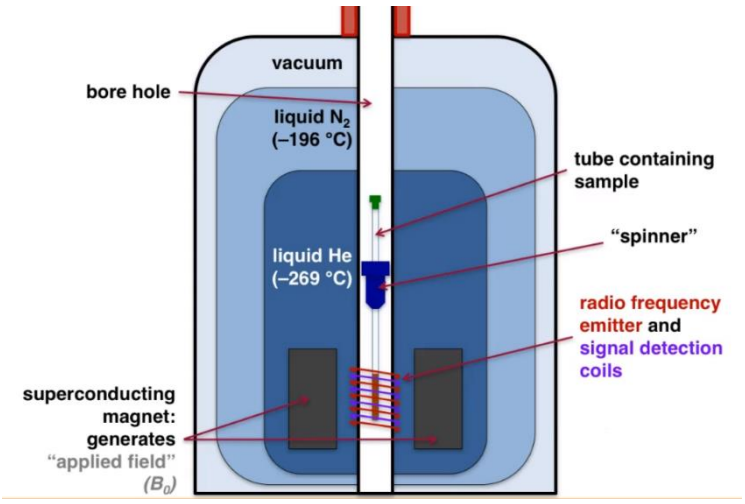

Figure 3-3 (67) Representation of the inside of an NMR machine

an radio wave pulse that acts as a new temporary magnetic field, $B_{1,}$ whose frequency corresponds to the Larmor frequency (angular frequency of the precessional motion in the magnetic moment). This results in the excess lower state nuclei converting to higher states of energy through absorption equal to the energy difference given by Bohr's equation and whose frequency corresponds to the resonance frequency. After some time, the excited state nuclei returns to its lower energy state, originating a current that is recorded by the signal detection coils originating at a peak in the NMR spectrum.

3.2 ATR FT-IR and ATR FT-IR microscopy

FT-IR is a very attractive technique widely used in fields such as chemistry, biology, and biochemistry has it provides the identification of molecules with a high signal-to-noise ratio and high resolution while giving spectra results that are analogous to fingerprints, meaning molecular structures can only give one infrared spectrum.(68, 69)

Depending on the molecular geometry, different molecules possess different molecular vibrations. In a nonlinear molecule, the number of ways a molecule can vibrate (*i.e.*, the number of *vibrational modes)* is given by $3N - 6$ degrees of freedom where 3N degrees of freedom are given by the translational motion and rotation motion over the *x*, *y* and *z*-axes.(70) In a linear molecule, the rotation about the axis of the bond does not involve any change of the position of the atoms, so one of the rotational degrees of freedom is lost thus possessing an additional vibrational state mode, displayed in $3N - 5$. Infrared spectroscopy derives from transitions

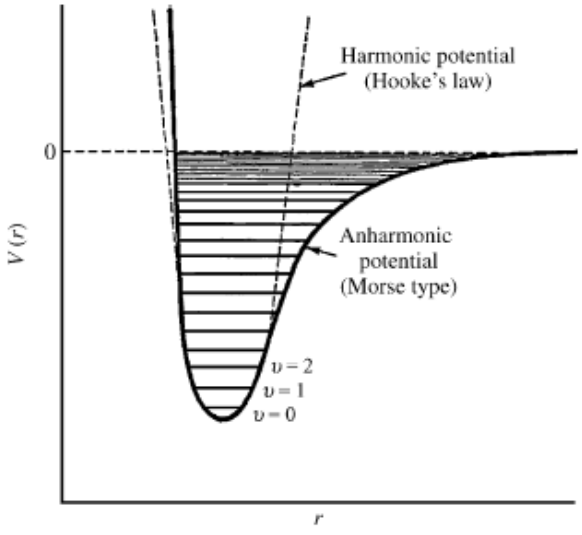

Figure 3-4 (70) Potential energy of a diatomic molecule as function of the atom's separation with quantized vibration quantum numbers displayed.

between quantized vibrational energy states (Figure 3-4). When the light absorbed by the atoms present in the sample reaches the energy difference necessary to transition between the ground state (υ=0) and first excited state (υ=1) the FT-IR detects the decrease in light intensity that was lost to the excited atoms giving a peak in the absorbance scale [This transition is where most vibrational modes are included and its radiation energy is in the mid-infrared spectrum (400 to 4000 cm^{-1})].(70) The absorbance of a sample is related to both the intensity of the background and sample spectrums and the concentration of molecules in a sample *via* Beer's Law.(71)

In ATR FT-IR, measuring a sample spectrum requires the use of radiation refraction (Figure 3-5).(71) The essence of this technique relies on Snell's law (equation 3-1) that describes the behaviour of radiation when passes from one transparent medium to another with different refractive index.(70)

Equation 3-1 Snell's law.

$$\eta_1 \sin\theta_1 = \eta_2 \sin\theta_2$$

Considering, η_1 the refractive index of the crystal, η_2 refractive index of the sample, Θ_1 and Θ_2 the angle of incidence and refraction incidence, according to this law, it is not possible to obtain total internal reflectance if $\eta_2 > \eta_1$. Furthermore, if we increase the angle of incidence, to a certain angle named critical angle, Θ_c, all incidence angles equal or superior to Θ_c will reflect internally as shown in figure 3-5. Despite contradictory, ATR FT-IR gives a spectrum of absorbance just like a "normal" FT-IR spectrum even though ATR is a reflectance technique.

By combining the mechanisms of infrared identification with microscope imagining, a new spectrum of applications can be used to uncover the composition of specific areas of the sample that it's being measured. The combination of two techniques is named hyphenated infrared techniques. In this case, a detector is used to draw the so-called molecular map in a grid pattern and within in the composition identification at specific spots chosen by the operator.(71)

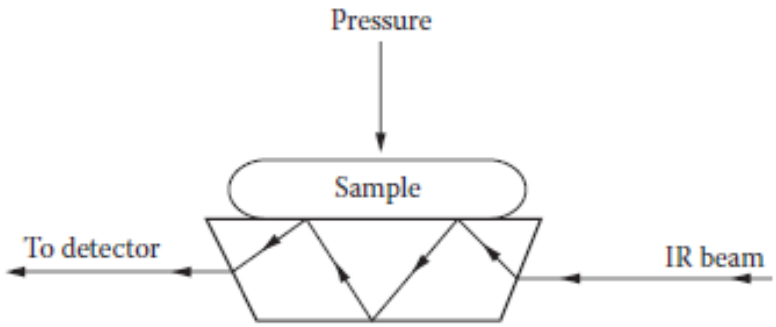

Figure 3-5 (70) ATR module work principle.

3.3 AFM

Since the invention of this technique, AFM has been a very useful tool to uncover surface morphology and chemical to physical properties of micron-to-nano structures at an atomic and subnanometer scale.(72)

AFM as a technique works by using a sharp tip to map the surface and has it feels the surface topology signals are sent *via* laser which is then reflected from the tip surface to a photo-detector (Figure 3-6). The feedback signals are sent to a signal processing software, which analyses and comprises a 2D or 3D plots.(72) Uncovering the surface topology can be made by contact mode where the tip is dragged along the surface or by tapping mode which vibrates the cantilever (object that holds the tip) at or near its resonance frequency to scan the surface. Despite the different methods used to "feel" the surface, the local height of a surface (surface morphology in AFM is made at each point, called pixel, of a 2D array that consists of the mapped surface) is determined by measuring the vertical or Z displacement needed to touch the surface.(73) Furthermore, although the principle of measuring the height of a sample is the same, different mechanics in function of the technique are used. Looking more in-depth to the tapping mode ability to measure the surface morphology, as it is the mechanism used in this work, this method tracks the surface topology *via* amplitude of the cantilever. A Z scanner displaces at each pixel the distance between the oscillating tip and the sample to keep the amplitude constant during surface measurements (Figure 3-7). To obtain clear images during these experiments, the quality of the data must provide high resolution for this effect and one factor that is crucial for this endeavour is the precise control of the tip-surface interactions. These interactions are based on

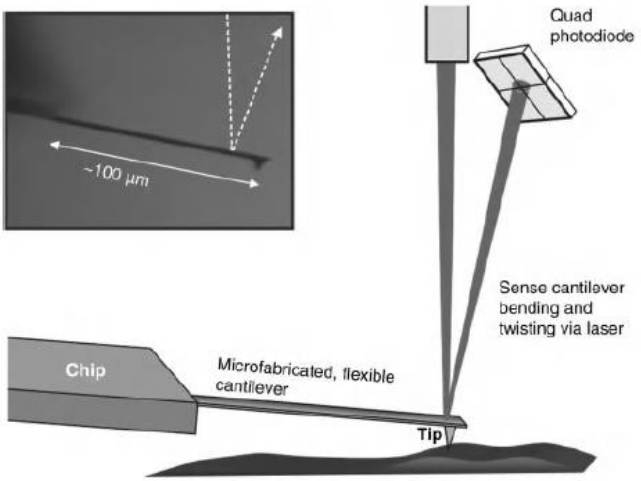

Figure 3-6 (73) Schematic representation of AFM procedure.

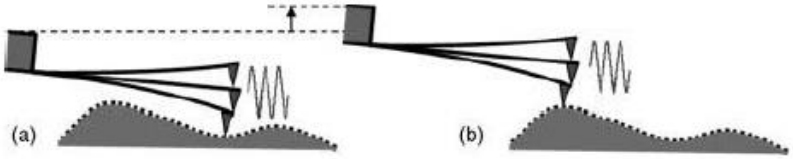

Figure 3-7 (73) AFM tapping mode mechanism.

continuum mechanics, long-range van der Waals forces, capillary forces, short-range forces, electrical double layer force in a liquid, and contamination effects.(72) Each force represents a different way that the tips interacts with the surface, and thus to produce a good atomic resolution image the tip must be able to counteract the tip-surface interactions described above.(72)

Chapter 4. Experimental methods

4.1 Materials

The following materials were purchased from Sigma-Aldrich, USA: 4 cyano-4-(phenyl-carbonothioylthio) pentanoic acid, CPAD, (>97%), 2,2′-Azobis (2-methylpropionamidine) dihydrochloride, VA-044, (97%), BIBB, (98%), pyridine (≥99%), copper(II) bromide, $Cu^{II}Br_2$, diethyl ether (DEE) (>99%), NIPAM (≥99), N,N,N',N'',N''-Pentamethyldiethylenetriamine, PMDETA, (99%), and all deuterated solvents for ^{1}H-NMR, except for chloroform-d, $CDCl_3$ which was acquired from Cambridge Isotope Laboratories (Inc., USA). HEMA (97%), also purchased from Sigma-Aldrich, was purified from the oxygen inhibitor (remove the monomethyl ether hydroquinone) by passing the polymerizable vinyl monomer through a basic alumina (Brockmann I activated grade from Sigma-Aldrich with 50-200 μm pore size range) and filtered through Whatman® SPARTAN® 30/0.2 RC syringe filters. Copper(I) bromide, $Cu^{I}Br$, was purchased from Sigma-Aldrich as well and it was purified in glacial acetic acid (anhydrous acetic acid). The greenish powder was stirred for at least 2 hours in acetic acid for 3 times. Afterwards, the salt was washed with ethanol. The salt finally was filtered, rinsed three times with ethanol and dried under vacuum overnight. The catalyst was stored in the dark and in nitrogen glove box. Premium grade, Ensure @, solvents namely, methanol (MeOH), ethanol, acetone and DMF, were obtained from Merck KGaA, GER and the remaining solvents THF, hexane, heptane, toluene, chloroform, were purchased from Biosolve Chimie SARL (all belonging to Analytical grade). All the water used was ultra-pure water dispensed through a Milli-Q system from Millipore Corporation, USA.

Auxiliary equipment for all reactions and experiments made include VWR Blue Nitrile powder-free disposable gloves and samples vials with snap-caps, BRAUN Sterican® needles, BD Discardit™ II syringes, Swann-Morton® surgical scalpel blade No.23, Eppendorf® epT.I.P.S., Greiner bio-one TM CELLSTAR® test tubes (to store the several inks produced), gold substrates (1x1cm^2) were cut from a silicon wafer coated with 100 mm sputtered gold (Au).

4.2 Molecular Characterization

^{1}H-NMR spectra were acquired by Bruker Ascend 400 MHz spectrometer in deuterated dimethyl sulfoxide (DMSO-d_6) or $CDCl_3$ solvent and ATR FT-IR spectra were measured with Bruker Alpha spectrometer and Bruker HYPERION 1000/2000 microscope to characterize the molecular composition of the analyte tested. Gold substrates used for ATRP macroinitiator deposition were clean for 30 min with oxygen SPI Plasma-Prep II. The viscoelastic properties of the produced inks were analysed with the Paar Physica UDS 200 spectrometer. MicroFab technologies Jetlab 4 system printer permitted the defined deposition of initiator layers onto gold. Inkjet printed ink drops of grafted ATRP macroinitiator in gold was observed with an Olympus BX60 microscope, using 5x, 20x and 50x objective lens. Specialty Coating Systems, Inc Spincoater® model P6700 series was to spin coat different inks in the gold substrate. Wettability of different inks were performed with contact angle measurements (CA) from DataPhysics contact angle system OCA. AFM instrument Molecular Force Probe 3D (MFP-3D, Santa Monica, CA) was used to map the topography of the gold substrates.

4.3 Equipment configuration

4.3.1 Rheometer

The rheology of the inks were evaluated under conditions that simulate those of DOD inkjet printing, using the rotational mode with parallel plate. Prior to any measurements, a zero-gap function must be implemented to establish the limit downward dislocation that the spindle has to do to touch the inferior plate. This function varies with the spindle used and, in our case, we used an MP31 (50 mm, 0º) spindle. A Peltier temperature controller allowed the quick temperature control for the measurements. The gap and temperature between the spindle and the plate used for the rheometer test were of 0.5 nm at 25ºC. After this procedure is made, the rotation of the spindle was stabilized for 0.5 min. The viscosities were measured by applying shear rate from 0.01 to 400 1/min with Ramp log data profile. This profile collected 100 points (measurement duration per point of 2 s) with points taken for 200 s.

4.3.2 Inkjet Printing

Inkjet printing was set to define pre-established patterns with different configurations at room temperature. A drop generator of 700 µm diameter with a 60 µm glass nozzle with a

piezoelectric crystal is applied an external electric load. A uniform waveform with a 1 µs rise time, varying dwell and pulses used, 1 µs fall was employed with an adjustable frequency to obtain the best drops for each ink varying between 450 and 500 Hz. Before any experiment nozzle purification was made with a solution of hydrogen chloride with demineralized water to clean the nozzle.

4.3.3 Spin coating

Uniformly grafting layers were prepared by rotating the sample at 2000 Hz for 1 min. To prevent sample displacement, the sample was put on a vacuum plate.

4.3.4 CA

Water contact values for the tested substrates were determined by adding a water drop to the surface and calculating the angle value of the generated droplet.

4.3.5 AFM

To analyse the height and roughness of the gold surfaces a silica cantilever 2 was used. After the cantilever was brought to its resonance frequency vibration, the drop was located and after calibrating the laser with the cantilever surface the experiments were performed with a scan size of 60 µs, scan rate 0.10 Hz at 15 µm/s. The amplitude was set at 19.53 mV with a frequency of 89.596 kHz.

4.4 Fabrication method

4.4.1 RAFT Polymerization of HEMA

Two 100 mL round-bottom flasks were used to perform the RAFT polymerization of the monomer HEMA (10 mL, 0.082 mol) and the chain transfer agent, CPAD (0.0229 g, 0.82 mmol), with VA-044 initiator (0.0133 g, 0.41 mmol), water (5 mL) and methanol (5 mL) solvent media in a different flask. Also, DMF (1 mL) was added to the RAFT polymerization solution an internal reference for the evaluation of the conversion *via* ^{1}H-NMR. The flasks were sealed with a rubber septum and degassed by bubbling with argon gas and stirred for approximately 30 min. Monomer-CPAD solution was transferred into the thermal radical initiator solution. The mixture was then

heated up to 45^0C. After the desired time, the polymerization was stopped by quenching and by allowing the reaction mixture to contact air. The precipitated polymer was purified 3 times by precipitating in DEE. Finally, the purified polymer was dried in vacuum until all solvent and unreacted monomer was removed as confirmed by ^{1}H-NMR and ATR FT-IR spectra. HEMA conversion was calculated comparing the integration areas of the monomer double bond between 6.07 and 5.62 ppm that will decrease as the monomer is converted. Purified 6th PHEMA is shown in appendix A and the solubility table for other PHEMA of different molecular weight is displayed in appendix B.

4.4.2 Preparation of PBIEM

A 0.397 g sample of PHEMA (-OH groups, 3.05 mmol) was dissolved in 4.90 mL of pyridine. Then 1.402 g (6.1 mmol) of BIBB was added dropwise at 0^{o}C in 60 min. The reaction mixture was left to stir at the same temperature for 3h followed by stirring at room temperature for 24 h. The insoluble salt was removed by filtration and the dissolved mixture was precipitated in hexane. The modified polymer was dried under vacuum. After ^{1}H-NMR analysis, an absolute quantitative conversion was obtained as shown in figure 5-4. PBIEM physical characteristics can be visualized in appendix C.

Chapter 5. Results and discussion

5.1 RAFT Polymerization of HEMA

RAFT polymerization technique was used to synthesise the ATRP macroinitiator. As described in the subchapter 1.2.2, polymer chain growth occurs when degenerative chain transfer between macro-RAFT agent and propagating radical take place so, kinetically, it is essential that the appropriate choice of RAFT agent is made regarding the monomer as the poor choice of this compounds, because the inherent nature of this polymerization, can lead from suppression of rate of polymerization to uncontrolled radical polymerization resulting in broad molecular weight polymers. For this reason, CPAD CTA (Scheme 5-1) was chosen as dithioesters are one of the most activated RAFT agents and usual choice to polymerize methacrylate monomers as is the case with HEMA.(74) Furthermore, the dithiobenzoyl group present in CPAD will play a critical role in the end-use application namely self-assembly monolayers in gold. A water-soluble with a low decomposition temperature azo initiator in VA-044 was chosen to initiate the radical polymerization by thermal decomposition. The procedure RAFT polymerization was carried out several times with the aim to evaluate the effect of the solvent on the length of the macromolecules (Table 5-1). Despite imploring different reactions mixtures, the same polymeric reaction temperature was established at 45ºC. Also, the [M]:[RAFT agent]:[Initiator] ratio was maintained

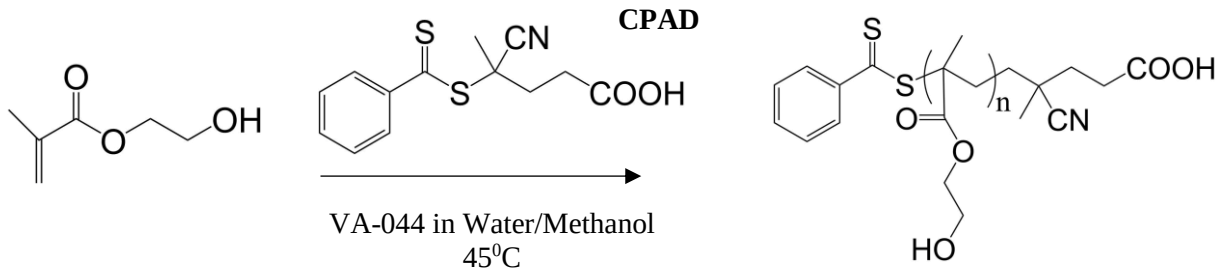

Scheme 5-1 RAFT polymerization of HEMA using CPAD as the CTA.

at [1000]:[1]:[0.5] with the monomer concentration being defined at 4.1M. The change of solvent was due to the loss of the control of the molecular weight of the synthesised polymer, *i.e.* it grew so much that the solution got so dense to the point of not be physically able to stir anymore.

Table 5-1 Characterization of PHEMA produced.

Experiences	Solvent	Time (minutes)	Conversion (%)	$^{a}M_{n,\ ^{1}H\text{-}NMR}$ $\times 10^{3}$
1	Water	120	39.2	50.99
2	Water:MeOH=1:1 v/v	180	58	75.47
3		45	14.6	18.96
4		45	12.0	15.55
5		60	17.1	22.19
6		60	17.7	23.09

[a]Theoretical Number-average molecular weight calculated as: $(\frac{\text{Conversion}\times[\text{M}]}{[\text{RAFT agent}]} \times \text{Monomer}_{\text{MW}})$

A probable cause may be connected to chemical cross-linking events after termination reaction. The selectivity of termination mechanism, suggests a recombination between active propagating chains, as it is reported for reactions of PMMA at higher temperatures.(75) Upon precipitation, the solution yielded two different colour polymer, namely bright pink and white. This contrast of colours may be attributed to the different conformations of the polymer chains formed. Since CPAD in solution has a pink colour, the precipitated white polymer must contain a higher molecular weight than the pink polymer because of linkage between different polymer chains which lowers even further the concentration of CAPD compared to the monomer concentration, making it negligible. The choice of the solvent used has a deep impact on the rate

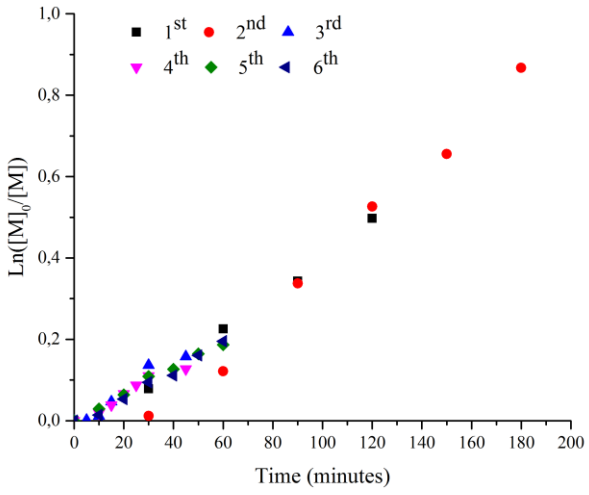

Figure 5-1 RAFT polymerization linear kinetic plots of HEMA.

constants of many homopolymerization reactions that contain monomers with hydroxy groups, such as HEMA.(15) Since water is a bad solvent for PHEMA, the probability of termination due to competing side reactions increase and controlled synthesis of the ATRP macroinitiator backbone proves more challenging as to just use a cosolvent that decreases the medium polarity slowing down the reaction to obtain better kinetics. Comparing the experiments obtained at the same time, namely at 45 and 60 minutes, similar conversions were achieved emphasizing the controlled nature of the chosen polymeric conditions. Linear kinetic semilogarithmic plots (figure 5-1) are shown that corroborate with the "living" polymerization mechanism of slow growth of living chains which are the opposite of FRP. The second experience shows an inhibition time until 30 minutes that can be explained by a delay in heating the reaction mixture to the predetermined value of 45^0C. Additionally, it is clear in all RAFT polymerizations the presence of an initial phase that has practically no polymerization conversion. This induction period that occurs, approximately, in the ten minutes of all reactions also can be explained by the heating of the reaction mixture, however, the concept of low reinitiation rate of the leaving group should also be considered.(76)·(77) Observing the conversion over time in accordance with the solvent choice, interesting results emerge, when at 45 min, every experiment besides the second one appears to have faster polymerizations rates which go against what is theoretically expected.

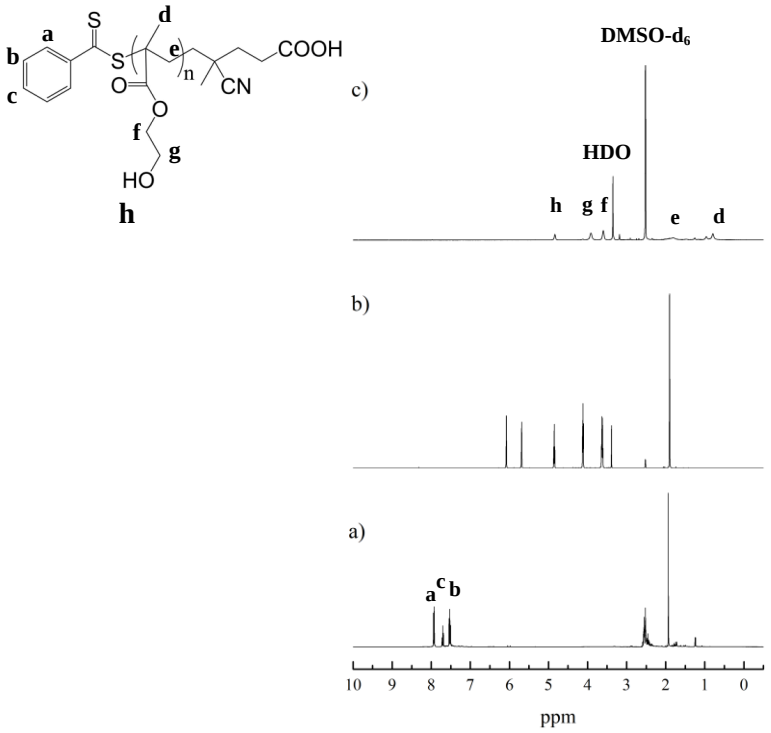

Figure 5-2 NMR spectra of CPAD (a), HEMA (b), 6th PHEMA (c).

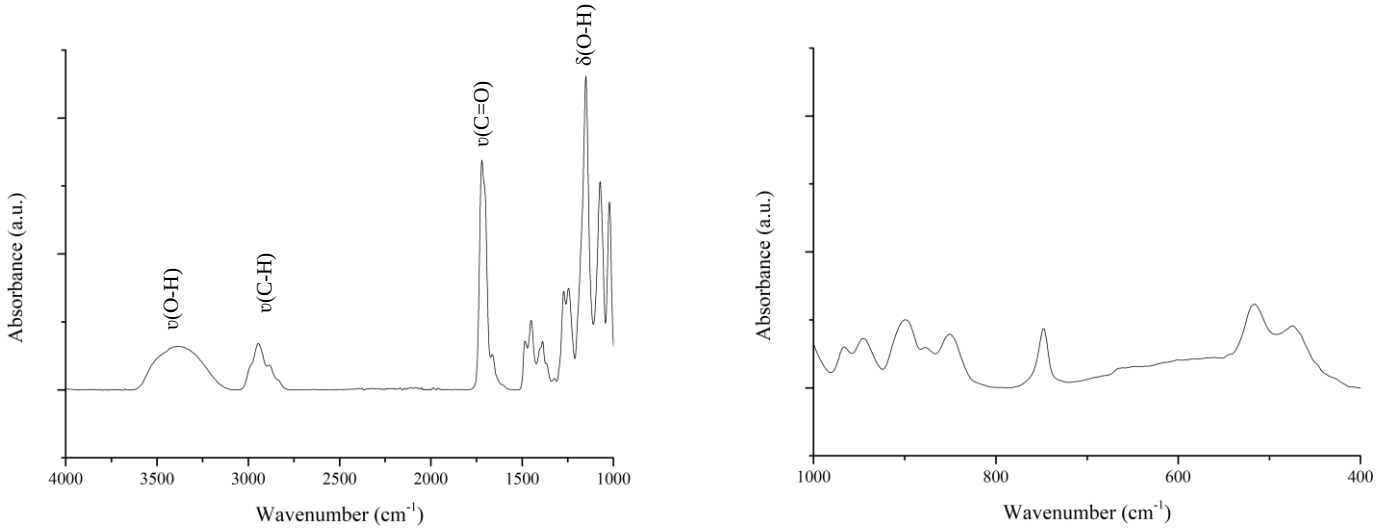

Figure 5-3 ATR FT-IR spectra of 6th PHEMA with highlighted characteristic peaks.

A reasoning for this contradiction derives from systematic data collection errors when obtaining conversions through the ^{1}H-NMR spectra. Figure 5-2 containing the ^{1}H-NMR spectra (DMSO-d_6; δ ppm) of 6th PHEMA displays the typical main chain polymer peaks at: 0.70-1.00 [3H, -CH3]; 1.90 [2H, -CH_2- backbone]; 2.52-2.53 DMSO-d_6 solvent signal; 3.19 [3H, -CH_3 from methanol]; 3.5 water peak; 3.56-4.16 [4H, -CH_2- from HEMA]; 5.21 [1H, -OH]. ATR FT-IR spectrum (cm^{-1}) for 6th PHEMA, displayed in figure 5-3 shows the characteristic absorption bands: 3390 cm^{-1}[υ(O-H)]; 2945 and 2882 cm^{-1}[υ(C-H)]; 1720 cm^{-1}[υ(C=O)]; 1152 cm^{-1}[δ(O-H)]. Additionally, the unreacted monomer band, 1634 cm^{-1} [υ(O-H)] does not appear further confirming the purity of the synthesised polymer.

5.2 Preparation of PBIEM

The preparation of ATRP macroinitiator active sites is discussed here. As it was said in the subchapter 1.2.3 ATR polymerization kinetics generally operates under persistent radical effect, where a transition metal complex traps the growing propagating radical chains in a deactivation process reaction. Because the composition of the dormant species consists of an initiating alkyl halide it is important that the latter reactive species be able to efficiently initiate an ATRP reaction for the selected monomer. In this sense, knowing different reactivity values of alkyl halides is crucial for appropriate initiator choice, especially for lower targeted DPn.(34) For the esterification reaction (Scheme 5-2), BIBB was chosen since it is a very common alkyl halide initiator precursor for ATRP due to high reactivity rate constant values.(16) PHEMA with different molecular weights were used to synthesize PBIEM (Table 5-2). Qualitative complete

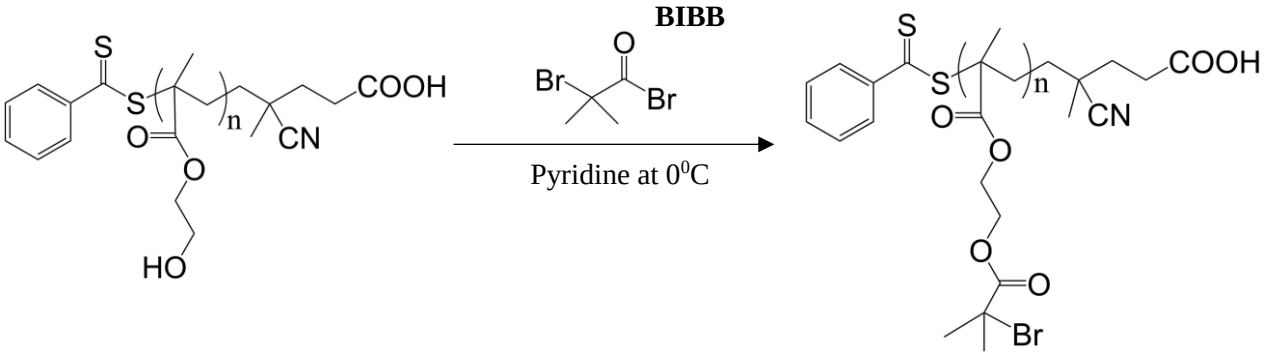

Scheme 5-2 Esterification reaction of PHEMA with BIBB

conversion was achieved in booth experiments as the methylene protons adjacent to the hydroxy group switch from 4.14-4.10 to 4.31-4.30 due to the difference of the methylene protons being adjacent instead to the ester group of PBIEM.(78) Because PHEMA was not dissolving in $CDCl_3$, comparative analyses on the shift of the methylene protons were made with HEMA NMR spectra. A representative ^{1}H-NMR and ATR FT-IR of PBIEM is displayed figure 5-4 and figure 5-5, respectively. The ^{1}H-NMR spectra ($CDCl_3$; δ ppm) of PBIEM can be observed: 0.70-1.00 [3H, -CH3]; 1.78 HDO solvent peak; 1.90 [2H, -CH_2- from the backbone and –CH_3 from BIBB]; 4.14-4.31 [4H; -CH_2 from HEMA]; 7.20 $CDCl_3$ solvent peak; Excess pyridine also appears after the solvent peak (Appendix D). Characteristic ATR FT-IR spectrum peaks (cm^1) for PBIEM are shown: 680 cm^{-1}[υ(C-Br)]. Observing the ATR FT-IR data of PBIEM originated from 1st PHEMA 51kda (PBIEM-A), 3416 cm^{-1} [υ(O-H)] region still appears in the spectrum. Being that all HEMA monomer was clean from the purified polymer, as it shows in figure 5-2, it is plausible to assume that total conversion was not achieved contrary of what has been reported by literature. This makes conversion confirmation extremely difficult because all PHEMA synthesised didn't dissolve in $CDCl_3$, eliminating the possibility of quantitative peak shift comparison. The solubility of the ATRP macroinitiator was tested to acquire information about possible ink solvents for inkjet printing (Appendix E).

Table 5-2 PBIEMs synthesised from PHEMA.

Experiment	ATRP macroinitiator backbone	Conversion %
1	6th PHEMA (22 kDa)	100%
2	1st PHEMA (51 kDa)	100%

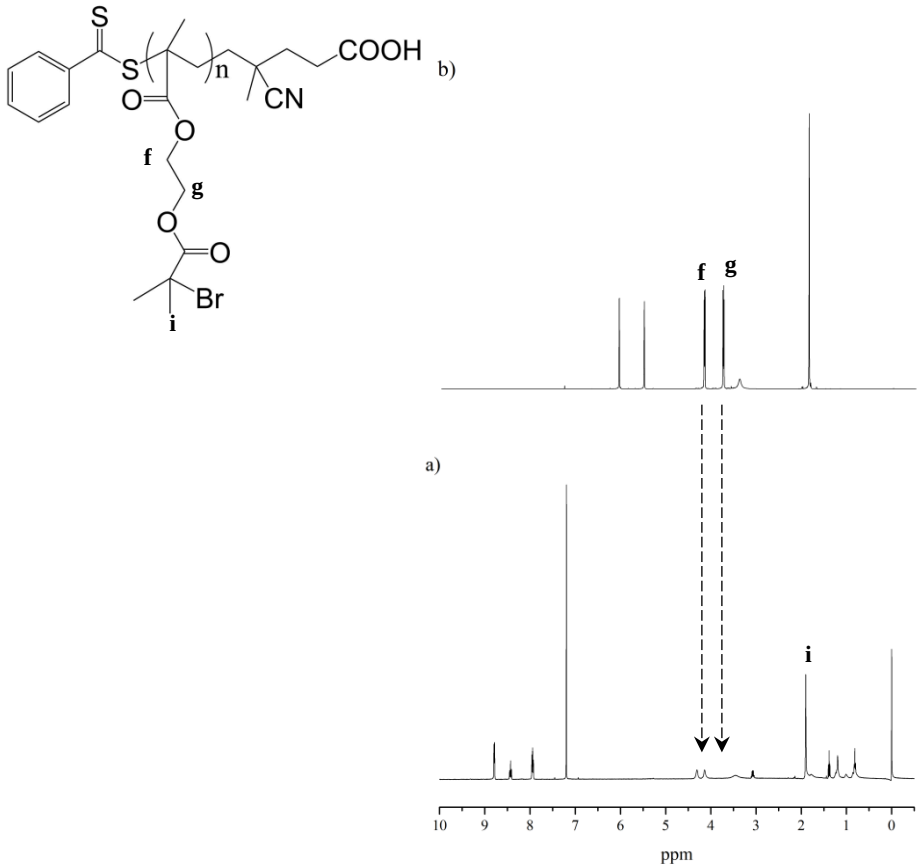

Figure 5-4 NMR of a) PBIEM-A, and b) HEMA in $CDCl_3$. Two dashed lines exhibit the shift of the methylene protons after BIBB coupling.

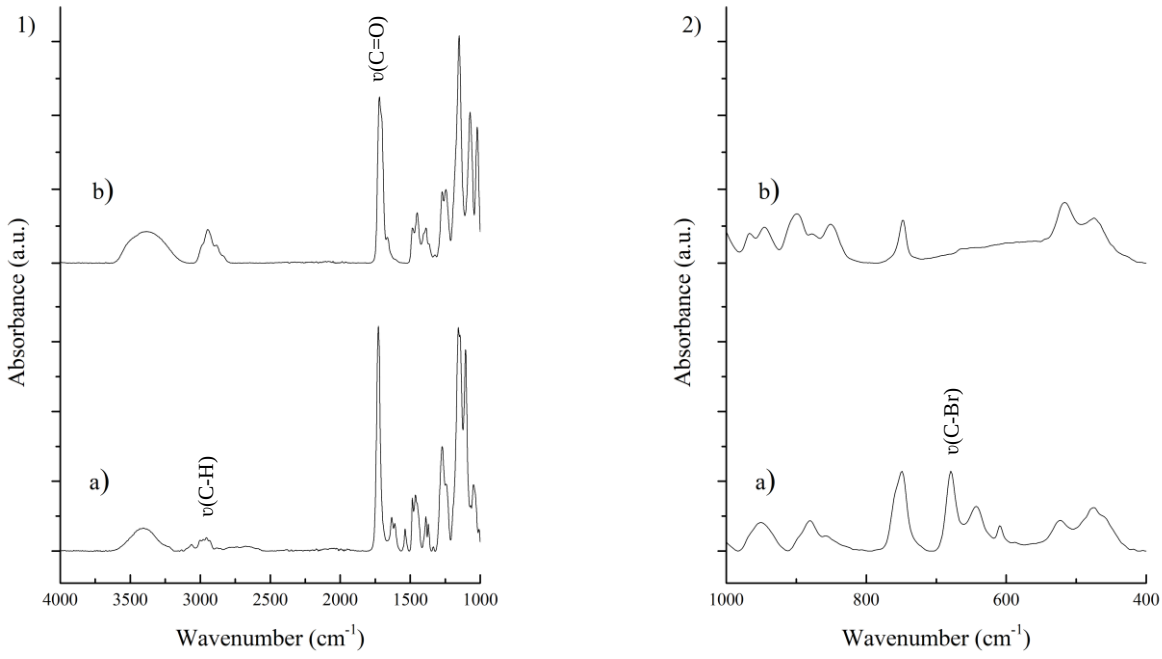

Figure 5-5 ATR FT-IR of a) PBIEM-A and b) PHEMA. Typical PBIEM peak is showcased in 2).

5.3 Inkjet Printing

In this section, printability factors, as described in the subchapter 1.2.4, namely as viscosity, wettability and surface tension were studied. The concept of self-assembly disulfide-gold monolayers will also be analysed as well as the probability of the end-group attachment to the gold surface in function of the macroinitiator length.

Several inks were made for inkjet printing with different compositions and concentrations (Table 5-3). Two different ATRP macroinitiator based inks containing PBIEM [PBIEM-A and PBIEM-B (from 6th PHEMA 23 kDa)], were grafted onto the gold substrate (scheme 5-3). The step height calculation of macroinitiator layers is shown in appendix F. DMF and acetone solvents were chosen to fabricate the several inks. Although 10% composition inks were produced with DMF, to be able to compare both inks, a concentration of 0.5% inks was synthesized as more volumes of acetone are needed to dissolve the ATRP macroinitiator. Average viscosity values range from 0.6 to 2.7 cP corresponding to PBIEM-A 0.5% in acetone and PBIEM-A 10% in DMF, respectfully. The overall ink viscosity values are relatively low compared to the normal range of printability of inkjet printers (1-25 cP) and this occurrence its explained, mainly, by the use of low viscous starting solvents to produce the ink.(44) However, good ink drops were still achieved for the more viscous inks, as is described more in depth afterwards. Under the same conditions, the percental increase of viscosity values its maximized by the ink composition and by the addition of higher molecular weight, which it is to be expected as polymer additives are commonly used in inks to modify ink properties such as viscosity (Table 5-4).(45) The viscoelastic behaviour of several inks is shown (Figure 5-6). When applied a shear stress to the inks produced, all inks displayed a constant ratio of stress to shear rate. This behaviour is typical of Newtonian flow model where the viscosity is independent of the shear rate.

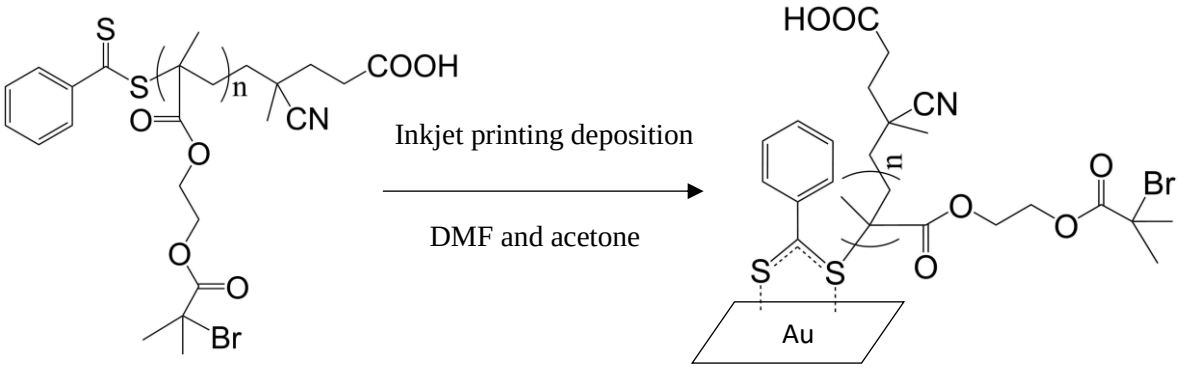

Scheme 5-3 Defined deposition of ATRP macroinitiator ink by inkjet printing.

Table 5-3 Different ink characterization and ATRP macroinitiator layer height.

Inks	ATRP macroinitiator	Solvent	[a]Composition % (w/w)	[b]Viscosity cP	[c]Droplet height nm
1	PBIEM-B	DMF	10	1.38	17±7
2			0.5	1.20	
3	PBIEM-A		10	2.7	
4			0.5	1.20	
5		acetone	0.5	0.6	

[a]Calculated using the formula: $100\times(mass_{PBIEM}/mass_{solvent})$.
[b]Average shear viscosity value.
[c]Value measured with AFM.

Table 5-4 Variable denomination for the ATRP macroinitiator, solvent and composition.

Variables	A+	A-	B+	B-	C+	C-
	PBIEM-B	PBIEM-A	DMF	acetone	10%	0.5%

Table 5-5 Viscosity percentual increase dependency.

Variables (x)	[a]Percental increase
$A^{+}B^{+}C^{x}$	15%
$A^{-}B^{+}C^{x}$	125%
$A^{x}B^{+}C^{+}$	96%
$A^{x}B^{+}C^{-}$	0.42%
$A^{-}B^{x}C^{-}$	93%

[a]Calculated with the following formula (%): $(x_{higher\ value}-x_{lower\ value})/\ x_{lower\ value}\times 100$.

Figure 5-6 (bottom figure) shows a small increase in viscosity, which was caused by the small concentration value of the ink as it can give unreliable data. This plot displays a flow curve with 2 different tangent values that increase with shear rate, behaviour that similars a derivation from Newton-law called shear thickening. The possibility of this ink having a different flow model is dismissed as it was more likely to observe this pattern in suspensions and this happens when an ink concentration is such that has the capacity to sediment the polymer particles in the ink. Furthermore, the molecular weight never changed so, the transition between two forms of behaviour connected to critical molecular weight (sudden increase in viscosity) can be dismissed as well.

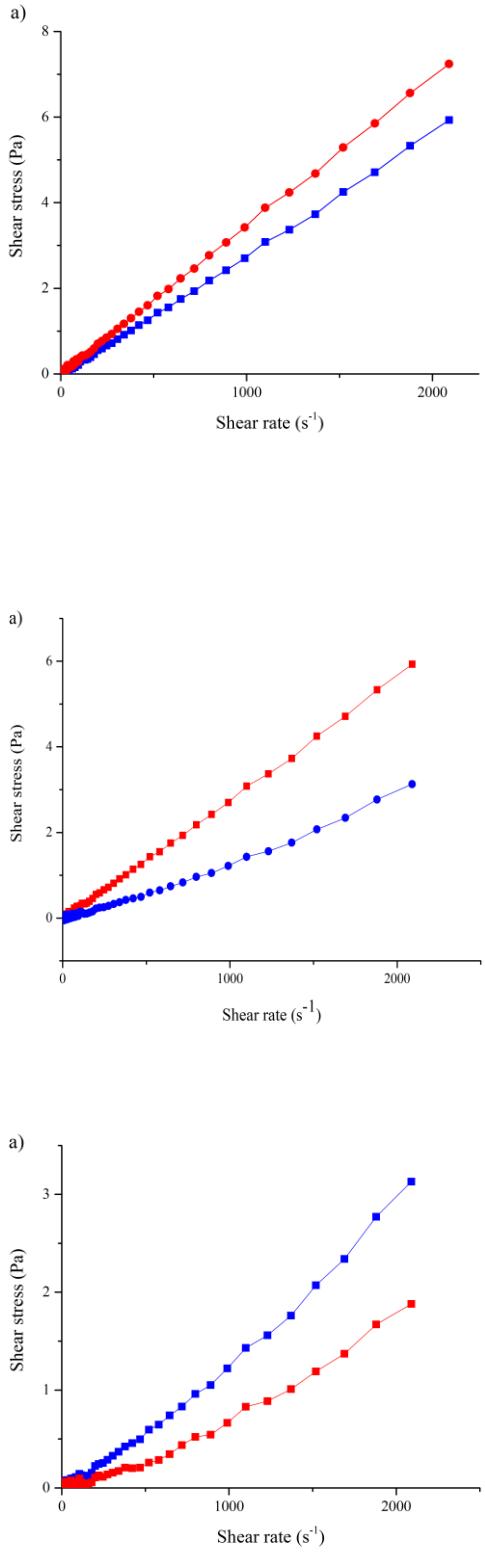

Figure 5-6 Graphic representation of some viscosity percentual increase combinations: PBIEM-A 0.5% in DMF (blue line) and in acetone (red line) (bottom figure), PBIEM-A DMF 10% (blue line) and 0.5 % (red line) (centre figure), 10% DMF PBIEM-B (blue line) and PBIEM-A (red line) (top figure).

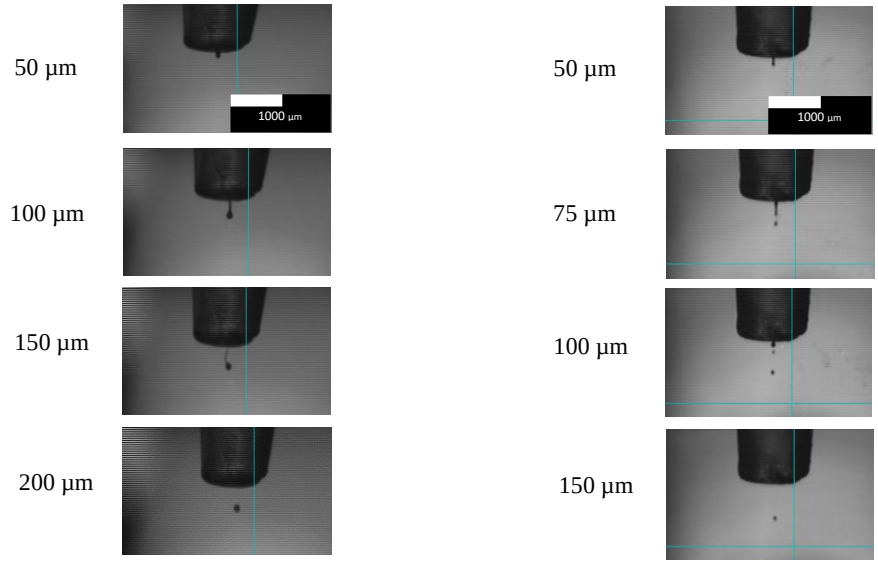

Figure 5-7 Drop formation of PBIEM-A 10% in DMF (a), and PBIEM-A 0.5% in acetone (b).

The practical difference in viscosity it's clearly demonstrated (Figure 5-7) where the filament rupture happens sooner in the less viscous ink. The low filament length and absence of satellite drops are correlated with Newtonian printing behaviour.(79) Upon printing, the shape of the droplet after the impact with the substrate was affected depending on which ink used. Experimental visualization of the droplet impact in the substrate is observed (Figure 5-8). Applying a more depth analysis visualization of the two different solvent inks, any of the DMF ink showed a more prominent capability to sustain the impact with the substrate in comparison with the acetone ink and thus having a more of a uniform shape throughout its total volume. The availability of producing define patterns with the inkjet printer is but a consequence of the ink produced, and in coating applications, the more uniform deposition inks would be more suited than more spread out deposition inks.(80) Ink droplets with a volume of 113 pL were achieved.

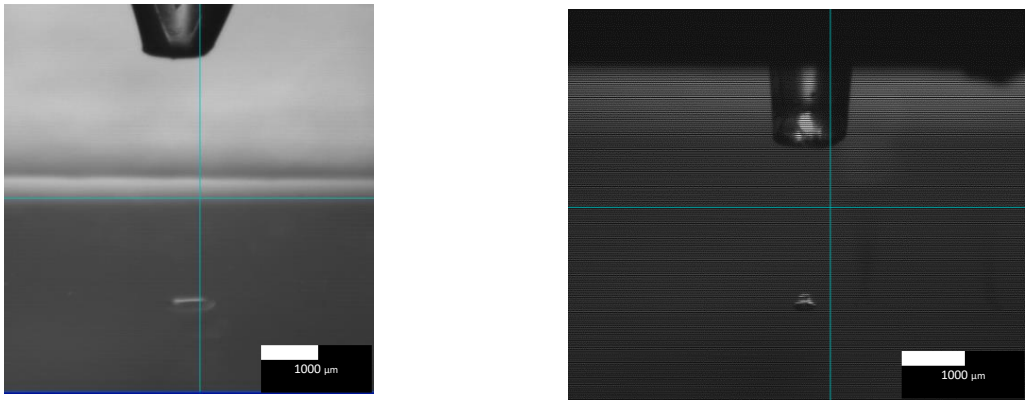

Figure 5-8 PBIEM-A 0.5% in acetone (left side) PBIEM-A 10% in DMF (right side).

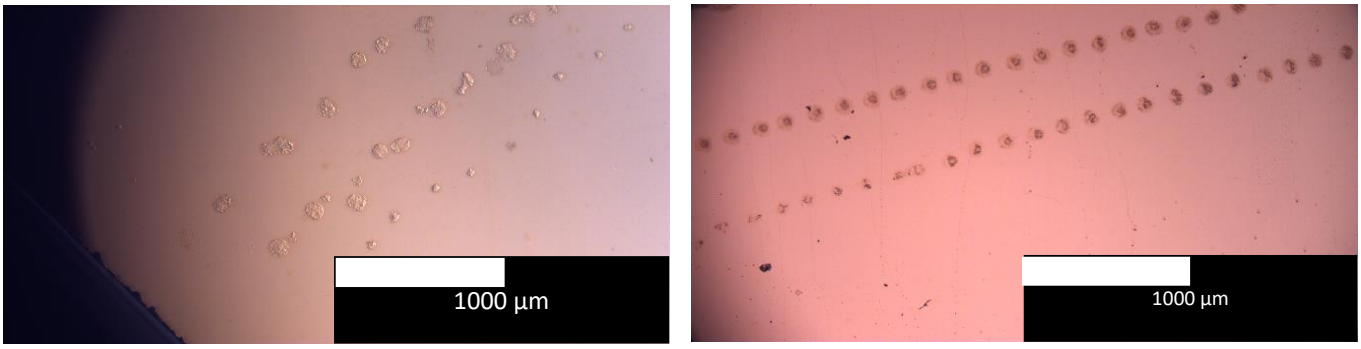

Figure 5-9 Pattern arrays of PBIEM-A 0.5% in acetone (left side) and PBIEM-A 10% in DMF (right side).

Using an optical microscope, well-defined patterns were visualized for most of the inks previously reported, figure 5-9, (settings in appendix G) except for some where overlapping or random conformation droplets were observed due in part the nozzle not being properly clean and, also, wrong configuration of printing settings either by the pulse or frequency applied (Appendix H). This is a scenario to avoid since it decreases the probability of polymer chains attaching to the substrate for the overlapping drops and reduces the precise droplet deposition which is a critical characteristic of this method. After washing the substrates, the only chains that remain attached are those that were capable to connect the dithiobenzoyl to the gold, in theory (Figure 5-10). The same figure also shows the resulting shape of the ink droplet after washing the substrate with DMF. Besides X-ray photoelectron spectroscopy (XPS) there is no true way to determine the amount of ATRP macroinitiator that is covalently grafted, only comparing visually both substrates that we can have an indication of the backbone influence as described previously. In my experience, the increase of the ATRP macroinitiator backbone reduces significantly the amount of graft polymer chains since the number of ink droplets that remains attached to the gold

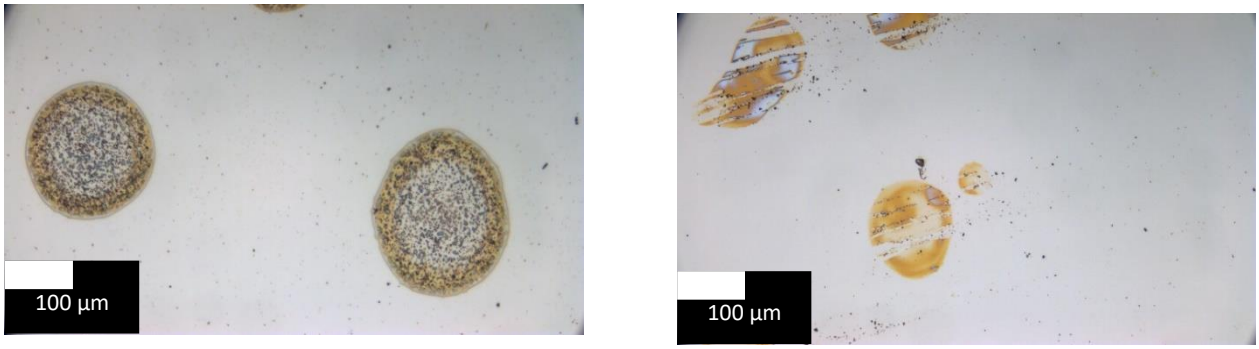

Figure 5-10 Optical microscope images of PBIEM-B 10% in DMF deposit ink droplets before (left side) and after washing (right side). On the left, a typical dewetting of the ink and the right visible scratches caused during the handling and the washing of the samples is shown.

after cleaning was substantially less. Of all inks produced, the PBIEM-B 10% in DMF proved to have the best grafting macromolecules after cleaning ratio (figure 5-11). Another critical visual effect observed in some inks deposits was the coffee-ring effect, as displayed in (Figure 5-10). This effect is observed when a non-uniform evaporation flux in a liquid-gas interface (surface tension gradient) or a thermal-induced gradient induces a capillary flow of suspended particles in a droplet and the Marangoni flow which governs the internal flow in a droplet (it's the key factor for the appearance of the coffee stain effect).(80) This appearance of this effect in some deposit inks is unexpected since polymer contained in the ink is completely dissolved. Besides optical microscopy contact angle measurements were also used to measure the difference in wettability of clean and grafted as another way to prove the presence of deposit ATRP macroinitiator. Exceptionally for this effect, spin-coated deposition method was used in a gold substrate with the 4^{th} ink and the 5^{th} ink produced. Starting with a gold substrate with a contact angle of $<10^{o}$ modified substrates with 61.3^{o} +/- 3 for 4^{th} and 57.0^{o} +/- 5 for the 5^{th} ink. Finally, infrared microscopy was used to prove the presence of ATRP macroinitiator grafted to the gold surface in comparison by comparison with the clean gold (Figure 5-12). Shifted typical PBIEM peak is displayed at 750 cm^{-1} [υ(C-Br)]. Again, 3416 cm^{-1} peaks [υ(O-H)] also appear indicating the presence of possible unreacted monomer. Unfortunately, with this spectrum, it's not clearly observed the disulfide bond. Combining these three methods we can conclude that we have a covalent bond between the ATRP macroinitiator and the gold substrate.

Figure 5-11 Patterned ink drops constituted of PBIEM-B 10% in DMF.

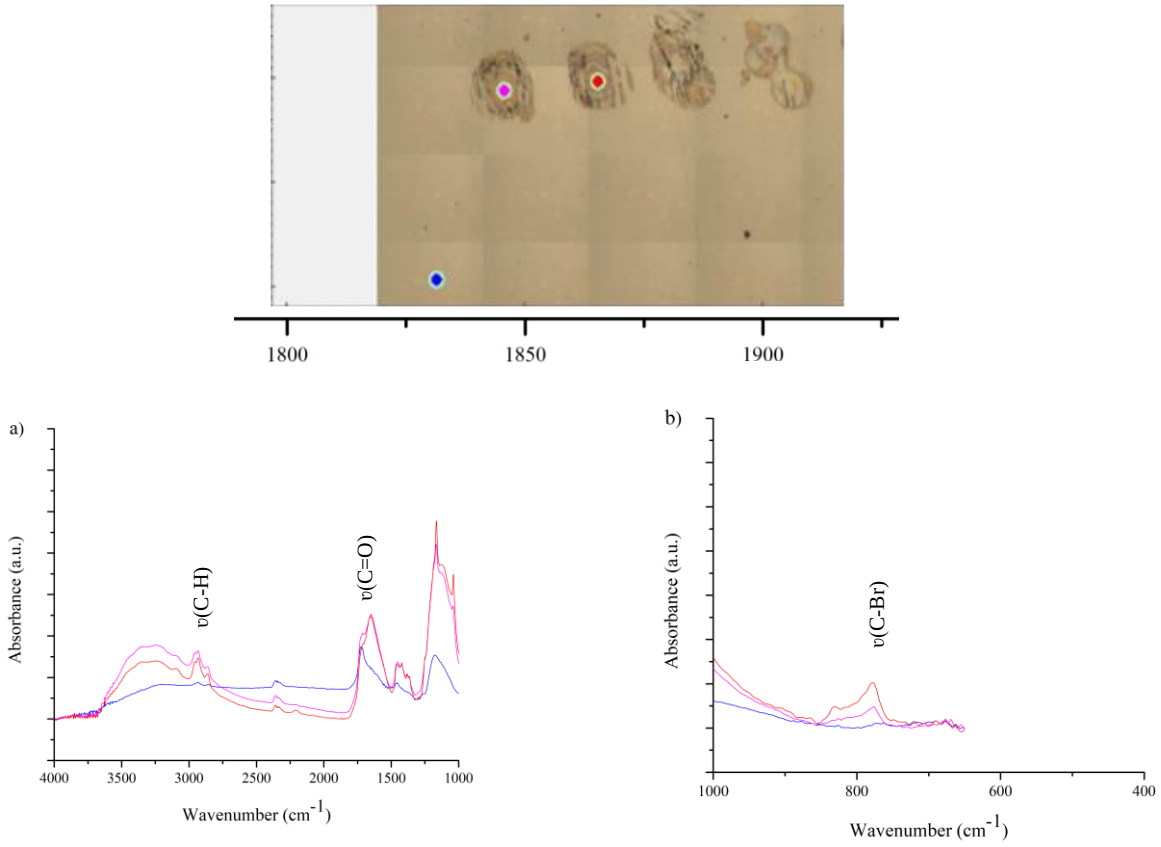

Figure 5-12 ATR FT-IR microscope spectra of PBIEM-B 10% in DMF and the molecular mapping imaging. Each dot colours gives a different spectrum with the same colour.

As a side note, it's interesting to note that the FT-IR microscopy spectra display much broader peaks compared to standard FT-IR which can be explained by sample size analysis where approximately 17 nm macroinitiator layers are being detected on a micrometre scale causing the peaks to become undifferentiated (the smallest proper measurable sample corresponds to the wavelength of mid-infrared radiation which is between 2.5 and 25 μm).(70)

Blank page

Chapter 6. Bottlebrush application

6.1 Introduction

Since its first synthesis in the early 1980s, bottlebrush polymers have been a topic of crescent interest (Figure 6-1) due to its unique and potentially useful properties that include high entanglement molecular weight, the self-assembly of bottlebrush block copolymer micelles in a selective solvent even at very low dilutions, and the functionalization of bottlebrush side-chains for recognition, imaging, or drug delivery in aqueous environments, as described by Verduzco et al.(81) Bottlebrush polymers can be synthesised *via* grafting from, grafting to and grafting through. For grafting from, this approach can produce very high bottlebrush backbones with controllable side chains grafting density as well as block copolymer side chains, despite the main drawback of this synthesis where functional groups often have to be protected and deprotected at each step.

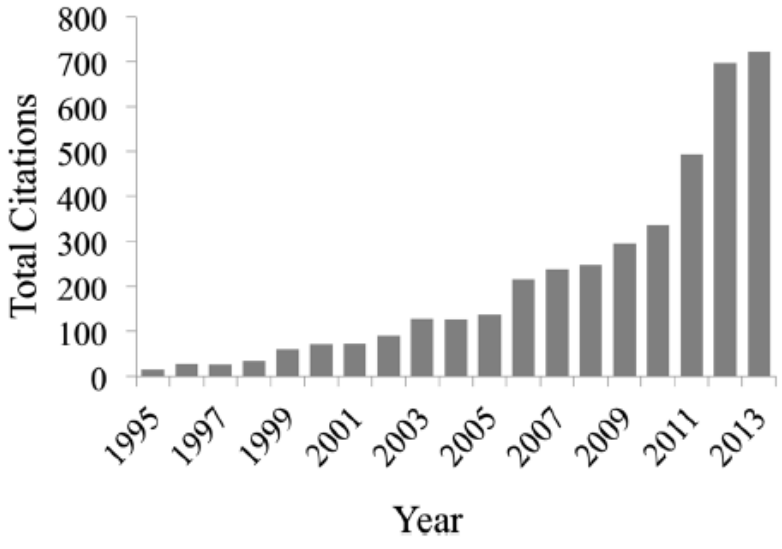

Figure 6-1 (81) Bottlebrush search results using the web of science.

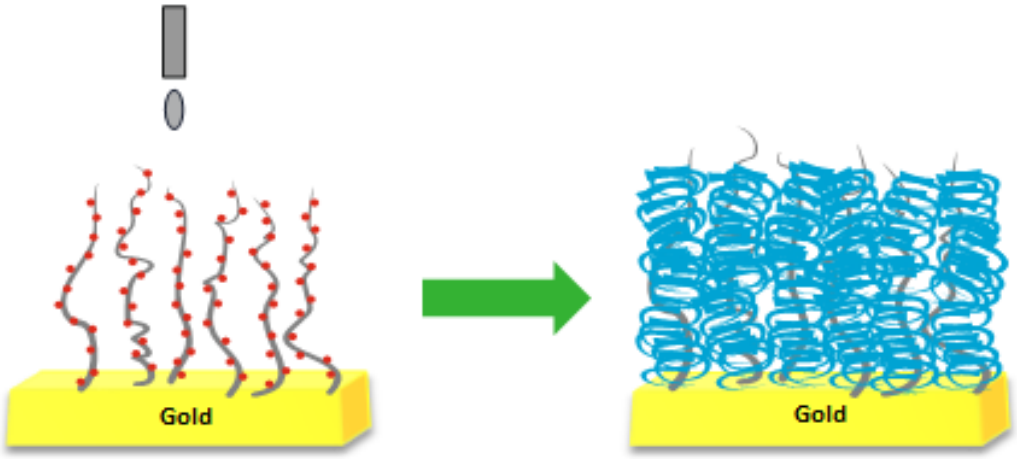

Scheme 6-1 Inkjet printing of ATRP macroinitiator (left side) with subsequent bottlebrush synthesis *via* grafting form.

Grafting to enables the separate and precise characterization of both backbone and side chains, however, it's not been widely used, since it produces bottlebrush with low grafting densities and as it happens with grafting through, low reactivity of polymeric reagents and difficult coupling reaction as a result of steric hinderance interactions between side chains.(81, 82) Grafting trough provides full grafting density of the backbone with a very simplistic method, despite reported unreacted macromonomer being hard to remove from the final product.(81) As in the work performed, grafting from an ATRP macroinitiator is displayed in figure 6-2.

6.2 Preparation of bottlebrush

First, five 50 mL flasks containing different compounds were prepared separately. In the first two flasks NIPAM (2.7 g, 0.238 mol), PMDETA (34 µL, 0.238 mmol) were dissolved in 30 mL of acetone. In the third flask, $Cu^{I}Br$ (11.4 mg, 0.079 mmol) and $Cu^{II}Br_2$ (1.8 mg, 0.0079 mmol). In the fourth flask, PBIEM (66 mg, 0.238 mmol) was dissolved in 10 mL of acetone. The fifth flask contained an inkjet printed grafted to gold ATRP macroinitiator. All flasks were sealed with a rubber septum and degassed by bubbling with argon and stirred for approximately 30 min. Materials from the first flask were added to the second flask. This intermediate solution was then transferred to the remaining flasks (the fourth and fifth flask, respectfully). The two solutions were put in an ice bath and left stirring for 24 h. Synthesised bottlebrush in solution was precipitated by drying in N_2 and its characterization was performed using ^{1}H-NMR. Grafted from bottlebrush copolymers were extracted from the solution dried in N_2 and its composition was verified by ATR FT-IR microscope. Bottlebrush present in solution after precipitation is shown

in appendix I. The conversion of bottlebrush side chain mas made by calculating the decrease of the monomer double bond, CH_2=CH between 5.5-6.5 ppm (Appendix J)

In the second method of producing PNIPAM bottlebrush side chains, 1.41 g (12.46 mmol) NIPAM, 18.4 mg (0.12 mmol) Cu^IBr, 79.1 µl (0.378 mmol) PMDETA in 20 mL of acetone, 35 mg (0.12 mmol) PBIEM in 10 mL of acetone and grafted PBIEM in 10 mL of acetone were placed in four 50 mL flasks under dry argon and stirred for 1 hour at room temperature (the first two monomer flasks had the same composition). After degassing, the monomer flask was added to the remaining flasks, put in an ice bath for 24h under stirring. Precipitation and characterization were the same as the method described before.

6.3 Results and discussion

An example of a final possible application, the synthesis of a stimuli-responsive monomer was chosen to produce the side chains of the bottlebrush. Monomer NIPAM chosen as the homo side chain polymer as is one of the most widely studied in stimuli-responsive polymers due to the lower critical solution temperature, LCST, (Temperature above which such polymers become insoluble due to a change in volume conformation) of ≈ 32ºC in water, meaning that visual confirmation of successful bottlebrush synthesis is easily obtained.(83)

Two different polymerization methods as described in subchapter 6.2 were utilized for bottlebrush fabrication. Exact conditions of this polymerization were not found in the literature (Table 6-1) so slight changes to the procedure, namely the solvent used in the reaction mixture, had to be implemented as booth literature recipes used a bad solvent, THF, relatively to all ATRP macroinitiators produced and thus to be able to dissolve them, acetone was chosen.

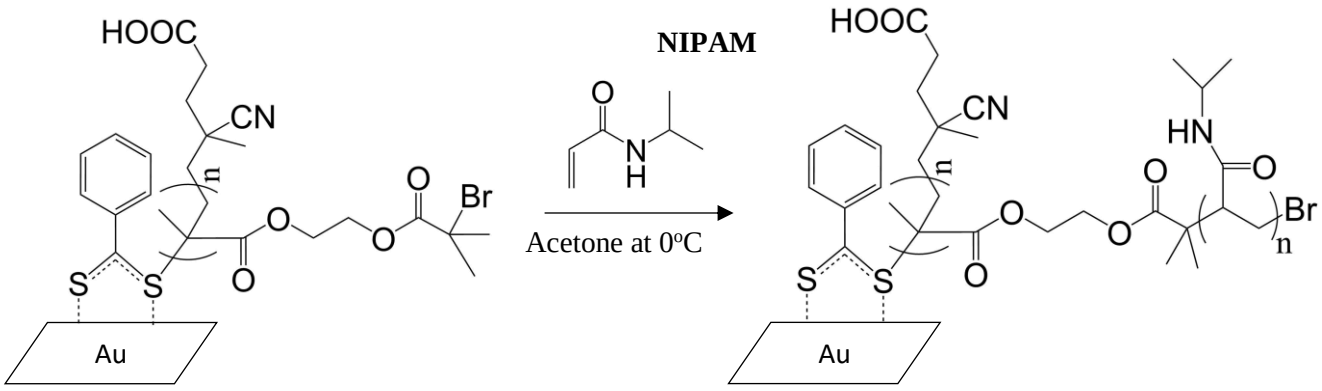

PBIEM **PBIEM-g-PNIPAM**

Scheme 6-2 Bottlebrush side chain synthesis by ATRP of NIPAM

Table 6-1 ATRP of NIPAM from the ATRP macroinitiator characterization.

Experiment	Deposit Ink Composition	Time (h)	Conversion (%)	$^{a}M_{n,\ ^{1}H\text{-}NMR}$
1	PBIEM-B 10% in DMF	1	2	226
2	PBIEM-A 10% in DMF	24	15	1697
	PBIEM-A 0.5% in acetone			1697

[a]Conversion formula is given as: $\text{Monomer}_{MW} \times \frac{\text{Conversion} \times [M]}{[PBIEM]}$

ATRP fractions conditions [M]:[PBIEM]:[$Cu^{I}Br$]:[$Cu^{II}Br_2$]:[Ligand] were [300]:[3]:[1]:[0.1]:[3] for the first procedure and [100]:[1]:[1]:[-]:[3] for the second procedure. The solvent influence in ATRP reactions is very substantial on the polymerization constant rates and its effect is verified in both experiences but particularly in the first experience which resulted in the need to change the method due to the very low grafted side chains conversion. The ATR FT-IR microscope spectra (cm^{-1}) for the first bottlebrush poly(PBIEM-graft-PNIPAM) (PBIEM-*g*-PNIPAM) shows the characteristic secondary amine absorption bands that belong to the NIPAM monomer: 1600 cm^{-1}[υ(N-H)]. Besides the 2% NIPAM side chain conversion another interesting occurrence in the first experience was the incapability to precipitate the bottlebrush present in solution with the following solvents: Water, ethanol, methanol, chloroform, DEE, toluene, hexane, heptane. As it happened in the first experience, the second polymerization revealed to be hard to precipitate as well. The second polymerization also revealed something interesting and that was, by mistake degassing of the $Cu^{I}Br$ containing flask was not properly done and as a result, a blue colour solution appears (Typical colour of the deactivator, $Cu^{II}Br$). When this flask was added to the ATRP macroinitiator flask, the solution turned instantly to green, signifying the presence of $Cu^{I}Br$. For that to happen some reduction had to take place and a possible reducing agent was the ATRP macroinitiator end-group (After oxidation the dithiobenzoyl group converts to disulfide).

Again, after bottlebrush synthesis, ATR FT-IR microscope was used to characterize the modified substrates. However, neither substrate showed the bottlebrush spectra. The spectra of the expected bottlebrush were the same as the spectra to clean gold. This appears to be a contradiction because if the substrate modified with PBIEM-B with 2% conversion has a differentiated spectrum at least the PBIEM-A with 15% conversion should also appear. An explanation for this event comes from the probability of disulfide-gold immobilization as referred in subchapter 1.1. Despite higher conversions or higher ATRP macroinitiator length, the actual layer density that is covalently grafted is smaller and small enough to the device not give correct spectra. Furthermore, chain detachment due to steric stress during ATR polymerization could not be observed.

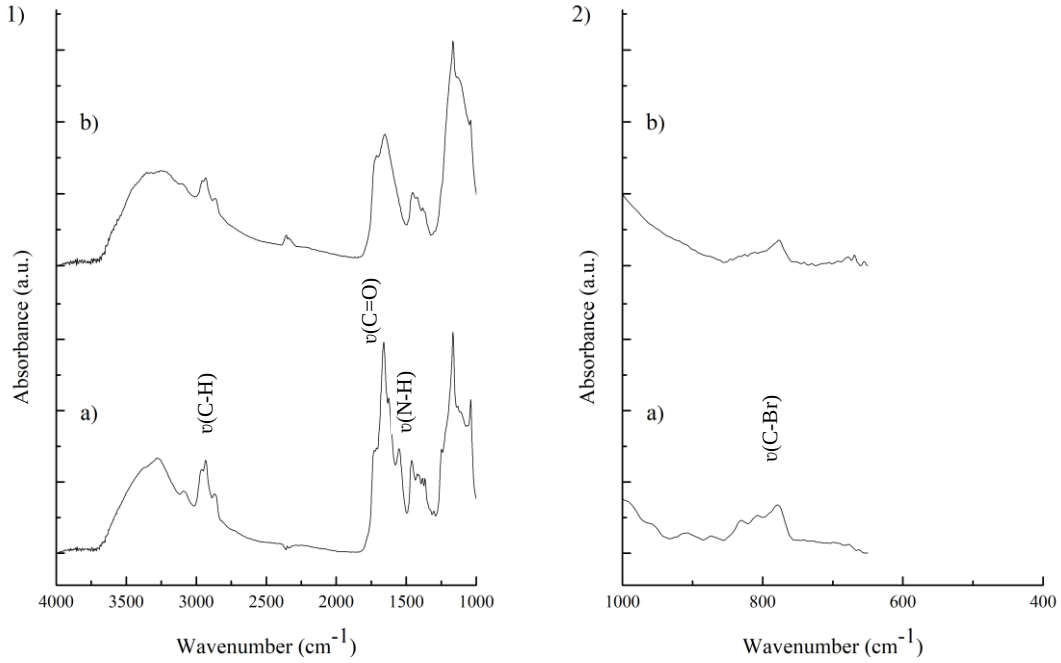

Figure 6-2 ATR FT-IR spectra of a) PBIEM-g-PNIPAM bottlebrush and b) PBIEM-A 10% in DMF.

Blank page

Chapter 7. Conclusion and recommendation

With inkjet printing, well-defined pattern arrays can be obtained, and its morphology is easily switchable digitally in accordance with the customer demand. In this report, patterned inkjet printed ATRP macroinitiators layers on gold were assembled for possible coating applications.

Successful ATRP-macroinitiator based on PHEMA was achieved by RAFT polymerization. The polymerization reaction was optimized to prevent loss of control relative to the molecular weight by changing the solvent used. Targeted molecular weights of 22 kDa and 51 kDa were used for coupling reaction with BIBB to yield and ATRP macroinitiator with absolute quantitative conversion according to literature but with probable lower conversion due to the presence of monomer typical hydroxy groups observed in ATR FT-IR.

Using inkjet printing and spin-coating, the covalent bond between gold surface and ATRP-macroinitiator *via* disulfide-gold immobilization is demonstrated by washing with considerable amounts of good solvents toward the initiator to promote separation between grafted and non-grafted initiator chains, observing the change in wettability between clean and grafted gold substrates and with the comparison between the spectra of pure gold and ink drop deposition sites by ATR FT-IR microscopy.

Newtonian inks of DMF and acetone solvents were used to deposit well-defined patterns with the punctual case of overlapping and random deposition of droplets due to the nozzle not being properly clean and incompatible printing settings. The influence of ink viscosity in function of macroinitiator molecular weight, solvent and composition were investigated and the primary factor for ink viscosity dependency was the ink composition at a higher molecular weight of ATRP macroinitiator. Unexpectedly coffee-stain effect was also observed in some inks. Of all inks produced the PBIEM-B 10% in DMF yielded the best ink relatively to grafting ratio and relatively to layer density as showcased by ATR FT-IR microscope. Initiator layers with approximately, 17nm are reported.

Successful bottlebrush fabrication with ATRP in acetone of NIPAM side chains was demonstrated with a maximum conversion of 15% and thus a full synthesis and templating technique was achieved.

Recommendations towards modifying certain aspects of this work to further optimize the developed work already produced are the following: Lowering the molecular weight of the ATRP macroinitiator has several advantages that could be explored as it increases the solubility making possible to dissolve it in other solvents to originate new and more efficient inks and increases the probability of end-group attachment to the gold substrates due to less steric hindrance. In terms of monolayers self-assembled in gold, thiol-gold interactions is one most studied mechanism in this area. (84) In this project, disulfide-gold reaction was utilized instead of reducing the ATRP macroinitiator end-group with nucleophiles (aminolysis reaction).(85, 86) Bain et al.(87) proved that thiol had a competitive adsorption of ≈75:1 over disulfide on gold in an ethanol solution and concluded that this advantage possibility originates from smaller steric hindrance, lower activation entropy of adsorption or even different rates of conversion of the initially physisorbed species to the chemisorbed thiolate. If in a targeted application this factor becomes relevant, end-group transformation is recommended. Although effective, the way how the ATRP macroinitiator was conceived only permits the immobilization in gold surfaces. In order to make the ATRP macroinitiator more universal towards other surfaces, a copolymer backbone containing the initiator and dual functional anchoring groups, based on catechol (targeting metals, metal oxides, mica and polymer surfaces) and pyrene(targeting carbon-based materials) have been designed and reported, and its adaption to this work is highly interesting as it further increases possible final application and by consequence increases its market value.(88) Last, and with the highly complex and technical application that this work tries to explore, non-metal ATRP could be tested since contaminant present after a normal ATRP reaction could be impractical to use, especially in biomedical applications.

Chapter 8. References

1. de Gans B-J. Duineveld PC. Schubert US. 2004. Inkjet Printing of Polymers: State of the Art and Future Developments. Advanced Materials. **16**: 203-213.
2. Chen J. Alonzo Calderon J. Yu X. Hong K. Ivanov I. Lavrik V. Banerjee M. Rathore R. Sun Z. Li D. Mays JW. Sumpter BG. Kilbey II SM. 2013. Grafting density effects, optoelectrical properties and nano-patterning of poly(para-phenylene) brushes. Journal of Materials Chemistry A. **1**: 13426-13432.
3. Emmerling SGJ. Langer LBN. Pihan SA. Lellig P. Gutmann JS. 2010. Patterning of a Surface Immobilized ATRP Initiator with an Inkjet Printer. Macromolecules. **43**: 5033-5042.
4. Li X. Prukop SL. Biswal SL. Verduzco R. 2012. Surface Properties of Bottlebrush Polymer Thin Films. Macromolecules. **45**: 7118-7127.
5. Krishnan S. Weinman CJ. Ober CK. 2008. Advances in polymers for anti-biofouling surfaces. Journal of Materials Chemistry. **18**: 3405-3413.
6. Rosenhahn A. Schilp S. Kreuzer HJ. Grunze M. 2010. The role of "inert" surface chemistry in marine biofouling prevention. Physical Chemistry Chemical Physics. **12**: 4275-4286.
7. Król P. Chmielarz P. 2014. Recent advances in ATRP methods in relation to the synthesis of copolymer coating materials. Progess in Organic Coatings. **77**: 913-948.
8. Stuart MAC. Huck WTS. Genzer J. Mller M. Ober C. Stamm M. Sukhorukov GB. Szleifer I. Tsukruk VV. Urban M. Winnik F. Zauscher S. Luzinov I. Minko S. 2010. Emerging Applications of Stimuli-Responsive Polymer Materials. Nature Materials. **9**: 101-113.
9. Nath N. Chilkoti A. 2002. Creating "Smart" Surfaces Using Stimuli Responsive Polymers. Advanced Materials. **14**: 1243-1247.
10. Biggs CI. Walker M. Gibson MI. 2016. "Grafting to" of RAFTed Responsive Polymers to Glass Substrates by Thiol–Ene and Critical Comparison to Thiol–Gold Coupling. Biomacromolecules. **17**: 2626-2633.
11. Cimen D. Caykara T. 2015. Micro-patterned polymer brushes by a combination of photolithography and interface-mediated RAFT polymerization for DNA hybridization. Polymer Chemistry. **6**: 6812-6818.
12. Kumar A. Whitesides GM. 1993. Features of gold having micrometer to centimeter dimensions can be formed through a combination of stamping with an elastomeric stamp and an alkanethiol ''ink'' followed by chemical etching. Applied Physics Letters. **63**: 2002-04.
13. de Gans B-J. Schubert US. 2004. Inkjet Printing of Well-Defined Polymer Dots and Arrays. Langmuir. **20**: 7789-7793.
14. Moya A. Gabriel G. Villa R. Javier del Campo F. 2017. Inkjet-printed electrochemical sensors. Current Opinion in Electrochemistry. **3**: 29-39.
15. Moad G, Solomon DH. (2005) The Chemistry of Radical Polymerization (Second Edition). In *1 - Introduction*. (Elsevier Science Ltd, Amsterdam), pp. 1-9.
16. Braunecker WA. Matyjaszewski K. 2007. Controlled/living radical polymerization: Features, developments, and perspectives. Progress in Polymer Science. **32**: 93-146.
17. Matyjaszewski K. 2015. Controlled Radical Polymerization: State-of-the-Art in 2014. American Chemical Society. **1187**: 1-17.
18. Matyjaszewski K. 1996. Controlled radical polymerization. Current Opinion in Solid State and Materials Science. **1**: 769-776.
19. Matyjaszewski K. 1993. Ranking living systems. Macromolecules. **26**: 1787-88.
20. Greszta D. Mardare D. Matyjaszewski K. 1994. "Living" radical polymerization. 1. Possibilities and limitations. Macromolecules. **27**: 638-644.
21. Solomon DH, Ezio R, Cacioli (1985) P US 4 581 429, Chem. Abstr.
22. Georges MK. Veregin RPN. Kazmaier PM. Hamer GK. 1993. Narrow molecular weight resins by a free-radical polymerization process. Macromolecules. **26**: 2987-2988.
23. Nicolas J. Guillaneuf Y. Lefay C. Bertin D. Gigmes D. Charleux B. 2013. Nitroxide-mediated polymerization. Progress in Polymer Science. **38**: 63-235.

24. Brandts JAM. van de Geijn P. van Faassen EE. Boersma J. van Koten G. 1999. Controlled radical polymerization of styrene in the presence of lithium molybdate(V) complexes and benzylic halides. Journal of Organometallic Chemistry. **584**: 246-253.
25. Maria S. Stoffelbach F. Mata J. Daran J-C. Richard P. Poli R. 2005. The Radical Trap in Atom Transfer Radical Polymerization Need Not Be Thermodynamically Stable. A Study of the MoX3(PMe3)3 Catalysts. Journal of the American Chemical Society. **127**: 5946-56.
26. Kotani Y. Kamigaito M. Sawamoto M. 1999. Re(V)-Mediated Living Radical Polymerization of Styrene: ReO2I(PPh3)2/R−I Initiating Systems. Macromolecules. **32**: 2420-2424.
27. Matyjaszewski K. Wei M. Xia J. McDermott NE. 1997. Controlled/"Living" Radical Polymerization of Styrene and Methyl Methacrylate Catalyzed by Iron Complexes. Macromolecules. **30**: 8161-8164.
28. Teodorescu M. Gaynor SG. Matyjaszewski K. 2000. Halide Anions as Ligands in Iron-Mediated Atom Transfer Radical Polymerization. Macromolecules. **33**: 2335-2339.
29. Kato M, Sawamoto M, HigashimuraS T. 1995. Polymerization of Methyl Methacrylate with the Carbon TetrachloridelDichlorotris-(triphenylphosphine)ruthedum(II)/Methylaluminum Bis(2,6-di-tert-butylphenoxide) Initiating System: Possibility of Living Radical Polymerization1. Macromolecules. **28**: 1721-1723.
30. Uegaki H. Kotani Y. Kamigaito M. Sawamoto M. 1997. Nickel-Mediated Living Radical Polymerization of Methyl Methacrylate. Macromolecules. **30**: 2249-2253.
31. Wang J-S. Matyjaszewski K. 1995. Controlled/"living" radical polymerization. atom transfer radical polymerization in the presence of transition-metal complexes. Journal of the American Chemical Society. **117**: 5614-5615.
32. Chiefari J. Chong YK. Ercole F. et al. 1998. Living Free-Radical Polymerization by Reversible Addition−Fragmentation Chain Transfer: The RAFT Process. Macromolecules. **31**: 5559-5562.
33. Matyjaszewski K. (2003) Advances in Controlled/Living Radical Polymerization. In: Controlled/Living Radical Polymerization: State of the Art in 2002. Vol. 854. (American Chemical Society,Washington), pp 2-9.
34. Matyjaszewski K. 2012. Atom Transfer Radical Polymerization (ATRP): Current Status and Future Perspectives. Macromolecules. **45**: 4015-4039.
35. Moad G. Thang S. 2009. Living Radical Polymerization by the RAFT Process – A Second Update. Australian Journal of Chemistry. **62**: 1402-1472.
36. Boyer C. Bulmus V. Davis TP. Ladmiral V. Liu J. Perrier S. 2009. Bioapplications of RAFT Polymerization. Chemical Reviews. **109**: 5402-5436.
37. Moad G. Rizzardo E. Thang S. 2008. Radical addition-fragmentation chemistry in polymer synthesis. Polymer. **49**: 1079-1131.
38. Keddie DJ. Moad G. Rizzardo E. Thang SH. 2012. RAFT Agent Design and Synthesis. Macromolecules. **45**: 5321-5342.
39. Kato M. Kamigaito M. Sawamoto M. Higashimura T. 1995. Polymerization of Methyl Methacrylate with the Carbon Tetrachloride/Dichlorotris-(triphenylphosphine) ruthenium(II)/Methylaluminum Bis(2,6-di-tert-butylphenoxide) Initiating System: Possibility of Living Radical Polymerization. Macromolecules. **28**: 1721-1723.
40. Wang J-S. Matyjaszewski K. 1995. "Living"/Controlled Radical Polymerization. Transition-Metal-Catalyzed Atom Transfer Radical Polymerization in the Presence of a Conventional Radical Initiator. Macromolecules. **28**: 7572-7573.
41. Tang W. Tsarevsky NV. Matyjaszewski K. 2006. Determination of Equilibrium Constants for Atom Transfer Radical Polymerization. Journal of the American Chemical Society. **128**: 1598-1604.
42. Fischer H. 2001. The Persistent Radical Effect: A Principle for Selective Radical Reactions and Living Radical Polymerizations. Chemical Reviews. **101**: 3581-3610.
43. Matyjaszewski K. Fundamentals of an ATRP Reaction. [Online]. Available: https://www.cmu.edu/maty/chem/fundamentals-atrp/index.html. Accessed in 13-08-2018.
44. Shlomo Magdassi. (2010) The chemistry of inkjet inks. (World Scientific Publishing Company, Singapore).

45. Li J. Rossignol F. Macdonald J. 2015. Inkjet printing for biosensor fabrication: combining chemistry and technology for advanced manufacturing. Lab on a Chip. **15**: 2538-2558.
46. Sankhe AY. Booth BD. Wiker NJ. Kilbey SM. 2005. Inkjet-Printed Monolayers as Platforms for Tethered Polymers. Langmuir. **21**: 5332-5336.
47. Le HP. 1998. Progress and Trends in Ink-jet Printing Technology. Journal of Imaging Science and Technology. **42**: 49-62.
48. Janata M. Masař B. Toman L. et a.l. 2002. Multifunctional ATRP macroinitiators for the synthesis of graft copolymers. Reactive and Functional Polymers. **50**: 67-75.
49. Matyjaszewski K. Miller PJ. Kickelbick G. Nakagawa Y. Diamanti S. Pacis C. 2000. Organic-Inorganic Hybrid Polymers from Atom Transfer Radical Polymerization and Poly(dimethylsiloxane). American Chemical Society. **729**: 270-283.
50. Miura Y. Narumi A. Matsuya S. et al. 2005. Synthesis of well-defined AB20-type star polymers with cyclodextrin-core by combination of NMP and ATRP. Journal of Polymer Science Part A: Polymer Chemistry. **43**: 4271-4279.
51. Cheng C. Khoshdel E. Wooley KL. 2005. ATRP from a Norbornenyl-Functionalized Initiator: Balancing of Complementary Reactivity for the Preparation of α-Norbornenyl Macromonomers/ω-Haloalkyl Macroinitiators. Macromolecules. **38**: 9455-9465.
52. Liu Y. Klep V. Zdyrko B. Luzinov I. 2004. Polymer Grafting via ATRP Initiated from Macroinitiator Synthesized on Surface. Langmuir. **20**: 6710-6718.
53. Cabane E. Keplinger T. Künniger T. Merk V. Burgert I. 2016. Functional lignocellulosic materials prepared by ATRP from a wood scaffold. Scientific Reports. **6**: 31287.
54. Beers KL. Gaynor SG. Matyjaszewski K. Sheiko SS. Möller M. 1998. The Synthesis of Densely Grafted Copolymers by Atom Transfer Radical Polymerization. Macromolecules. **31**: 9413-9415.
55. Neugebauer D. Sumerlin BS. Matyjaszewski K. Goodhart B. Sheiko SS. 2004. How dense are cylindrical brushes grafted from a multifunctional macroinitiator?. Polymer. **45**: 8173-8179.
56. Venkatesh R. Yajjou L. Koning C. Klumperman B. 2004. Novel Brush Copolymers via Controlled Radical Polymerization. Macromolecular Chemistry and Physics. **205**: 2161-2168.
57. Fleet R. T.A. Van den Dungen E. Klumperman B. 2011. Synthesis of novel glycopolymer brushes via a combination of RAFT-mediated polymerisation and ATRP. South African Journal of Science. **107**: 1-11.
58. Mukumoto K. Li Y. Nese A. Sheiko SS. Matyjaszewski K. 2012. Synthesis and Characterization of Molecular Bottlebrushes Prepared by Iron-Based ATRP. Macromolecules. **45**: 9243-9249.
59. Zamfir M. Rodriguez-Emmenegger C. Bauer S. Barner L. Rosenhahn A. Barner-Kowollik C. 2013. Controlled growth of protein resistant PHEMA brushes via S-RAFT polymerization. Journal of Materials Chemistry B. **1**: 6027-6034.
60. Li X. Wang M. Wang L. et al. 2013. Block Copolymer Modified Surfaces for Conjugation of Biomacromolecules with Control of Quantity and Activity. Langmuir. **29**: 1122-1128.
61. Lutz J-F. 2011. Thermo-Switchable Materials Prepared Using the OEGMA-Platform. Advanced Materials. **23**: 2237-2243.
62. Jonas AM. Hu Z. Glinel K. Huck WTS. 2008. Effect of Nanoconfinement on the Collapse Transition of Responsive Polymer Brushes. Nano Letters. **8**: 3819-3824.
63. Jonas AM. Glinel K. Oren R. Nysten B. Huck WTS. 2007. Thermo-Responsive Polymer Brushes with Tunable Collapse Temperatures in the Physiological Range. Macromolecules. **40**: 4403-4405.
64. Lamber, JB and Mazzola, EP. (2004) Nuclear Magnetic Resonance Spectroscopy: An Introduction to Principles, Applications, and Experimental Methods. (Pearson Education Inc., New Jersey).
65. Harris, RK. (1986) Nuclear Magnetic Resonance Spectroscopy. (Longman Scientific & Technical, Harlow).
66. Akitt, JW and Mann, BE. (2000) NMR and Chemistry: An introduction to modern NMR spectroscopy. Fourth edition. (Stanley Thornes (Publishers) Ltd., Boca Raton).

67. Allwood, D. NMR Spectroscopy: Basic Theory. [Online]. Available: https://www.youtube.com/watch?v=T3scEom1E1s. Accessed in 15-09-2018.
68. Scientific T. Introduction to Fourier Transform Infrared Spectroscopy. [Online]. Available: https://tools.thermofisher.com/content/sfs/brochures/BR50555_E_0513M_H_1.pdf. Acessed in 14-09-2018.
69. Markovich, RJ and Pidgeon, C. 1991. Introduction to Fourier Transform Infrared Spectroscopy and Applications in the Pharmaceutical Sciences. Pharmaceutical Research. **8**: 663-675.
70. Griffiths, PR and Haseth, JA. (2007) Fourier Transform Infrared Spectrometry Second edition. (John Wiley & Sons, Inc., New Jersey).
71. Smith, BC. (2011) Fundamentals of Fourier Transform Infrared Spectroscopy. Second edition. (CRC Press, Boca Raton).
72. Gupta, V. (2012) Atomic Force Microscopy -Imaging, Measuring and Manipulating Surfaces at the Atomic Scale. In *Crystal Lattice Imaging Using Atomic Force Microscopy*, Bellitto, V. (Eds) (InTech, Salt Lake City), pp 1-18.
73. Haugstad, G. (2012) Atomic Force Microscopy: Understanding Basic Modes and Advanced Applications. (John Wiley & Sons, Inc., New Jersey).
74. Moad G. 2017. RAFT polymerization to form stimuli-responsive polymers. Polymer Chemistry. **8**: 177-219.
75. Nakamura Y. Yamago S. 2015. Termination Mechanism in the Radical Polymerization of Methyl Methacrylate and Styrene Determined by the Reaction of Structurally Well-Defined Polymer End Radicals. Macromolecules. **48**: 6450-6456.
76. McNaught, AD and Wilkinson A. (1997) Compendium of Chemical Terminology: IUPAC recommendations. (Blackwell Science Publications, Oxford).
77. Graeme M. John C. K CY. et al. 2000. Living free radical polymerization with reversible addition – fragmentation chain transfer (the life of RAFT). Polymer International. **49**: 993-1001.
78. Cheng G. Böker A. Zhang M. Krausch G. Müller AHE. 2001. Amphiphilic Cylindrical Core−Shell Brushes via a "Grafting From" Process Using ATRP. Macromolecules. **34**: 6883-6888.
79. de Gans B-J. Kazancioglu E. Meyer W. Schubert U.S. 2004. Macromolecular Rapid Communications. **25**: 292-296.
80. Seo C. Jang D. Chae J. Shin S. 2017. Altering the coffee-ring effect by adding a surfactant-like viscous polymer solution. Scientific Reports. **7**: 500.
81. Verduzco R. Li X. Pesek SL. Stein GE. 2015. Structure, function, self-assembly, and applications of bottlebrush copolymers. Chemical Society Reviews. **44**: 2405-2420.
82. Husseman M. Malmström EE. McNamara M. et al. 1999. Controlled Synthesis of Polymer Brushes by "Living" Free Radical Polymerization Techniques. Macromolecules. **32**: 1424-1431.
83. Smith AE. Xu X. McCormick CL. 2010. Stimuli-responsive amphiphilic (co)polymers via RAFT polymerization. Progress in Polymer Science. **35**: 45-93.
84. Ulman A. 1996. Formation and Structure of Self-Assembled Monolayers. Chemical Reviews. **96**: 1533-1554.
85. Willcock H. O'Reilly RK. 2010. End group removal and modification of RAFT polymers. Polymer Chemistry. **1**: 149-157.
86. Lima V. Jiang X. Brokken-Zijp J. J. Schoenmakers P. Klumperman B. Van Der Linde R. 2005. Synthesis and characterization of telechelic polymethacrylates via RAFT polymerization. Journal of Polymer Science Part A: Polymer Chemistry. **43**: 959-973.
87. Bain CD. Biebuyck HA. Whitesides GM. 2010. Comparison of Self-Assembled Monolayers on Gold: Coadsorption of Thiols and Disulfides[1]. Langmuir. **5**: 723-727.
88. Wei Q. Wang X. Zhou F. 2012. A versatile macro-initiator with dual functional anchoring groups for surface-initiated atom transfer radical polymerization on various substrates. Polymer Chemistry. **3**: 2129-2137.

Appendix

Appendix A - Purified 6th PHEMA achieve using RAFT polymerization

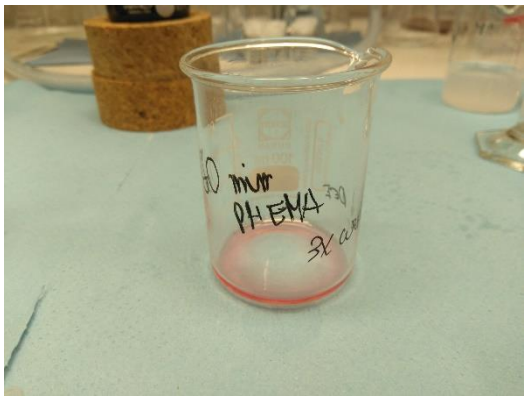

Appendix B - Solvent table for different synthesised PHEMA is displayed: The concentration test of the solubility test was:10 mg/mL. In the case of undissolved PHEMA, the concentration was diluted further to 10mg/ml+5ml.

Good solvent: Dissolved Bad solvent: Anything but a one-phase solution	1st PHEMA (51 kDa)	3rd PHEMA (19 kDa)
Acetone	Bad solvent	Bad solvent
Methanol	Good Solvent	Good Solvent
Iso-propanol	NA	Good Solvent
Water	Bad solvent	Bad solvent
DMF	Good Solvent	Good solvent
DMSO	Good Solvent	Good solvent
Chloroform	Bad solvent	Phase separation
Diethyl ether	Bad solvent	Bad solvent
THF	Bad solvent	Bad solvent
Toluene	Bad solvent	Phase separation

Appendix C - Purified PBIEM-B.

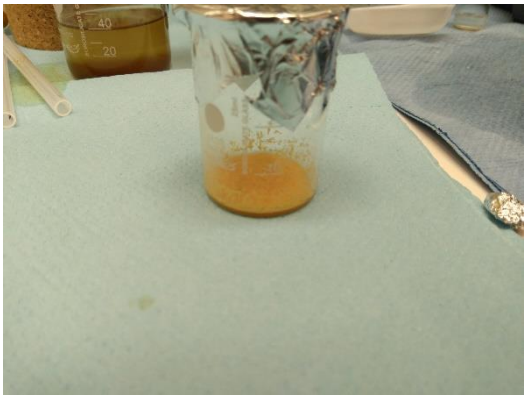

Appendix D – Pyridine NMR

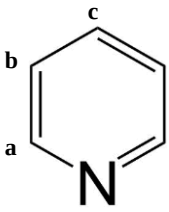

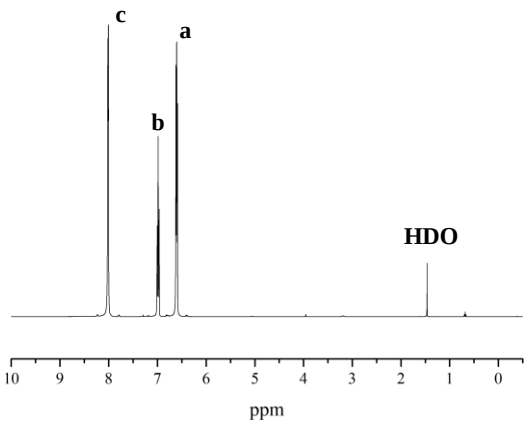

Appendix E - Solvent table for different fabricated PBIEM is shown: The concentration test of the solubility test was the same as the solubility test for PHEMA.

Good solvent: Dissolved Bad solvent: Anything but a one-phase solution	PBIEM-A	PBIEM-B
Acetone	Good solvent	Good solvent
Acetonitrile	Bad solvent	NA
Methanol	Bad solvent	Bad solvent
Iso-propanol	Didn’t dissolve completely	NA
Water	Bad solvent	Bad solvent
DMF	Good solvent	Good solvent
DMSO	Good solvent	Good solvent
Chloroform	Good solvent	Good solvent
N-hexane	Bad solvent	Bad solvent
Diethyl Ether	Bad solvent	Bad solvent
THF	Bad solvent	Dissolved partially
Toluene	Didn’t dissolve completely	Didn’t dissolve completely
Ethylene glycol	Bad solvent	Bad solvent

Appendix F – AFM step height determination.

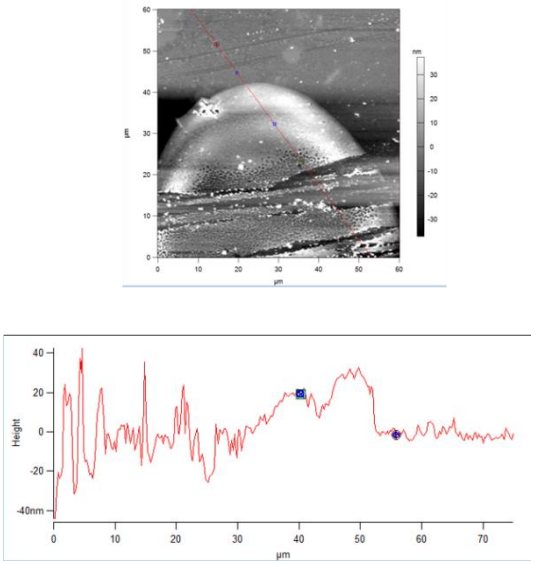

Appendix G- Inks produced and shown in the work. 1st setup: PBIEM-A 10% in DMF (left side); PBIEM-A 0.5% in acetone (right side).

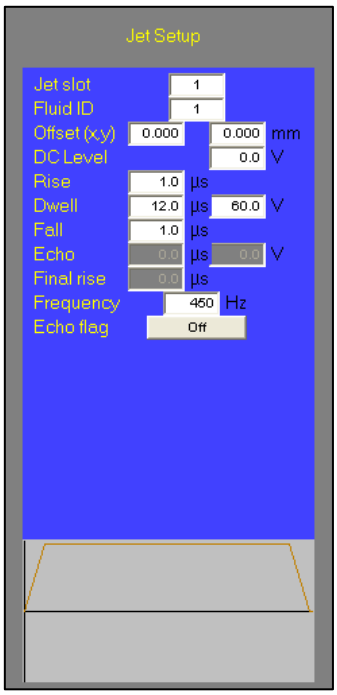

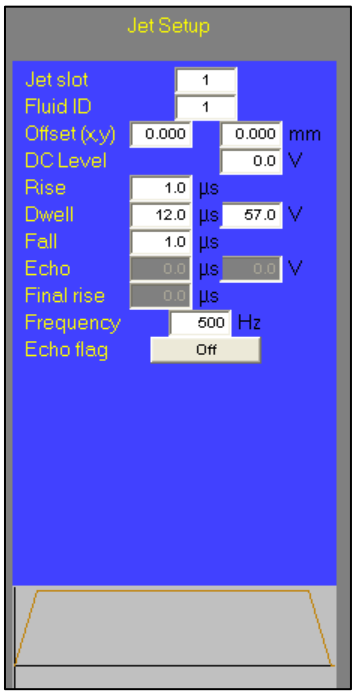

Appendix H – PBIEM-A 0.5% in acetone ink deposition and PBIEM-A 10% in DMF when bad settings for printing are used.

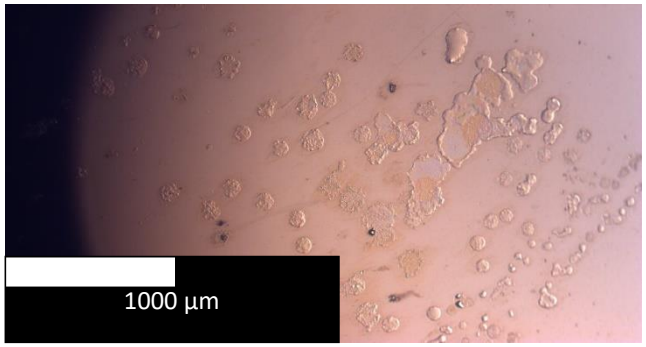

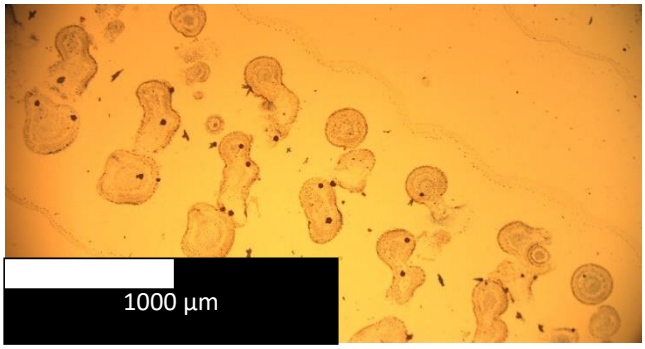

Appendix I – Precipitated bottlebrush present in solution.

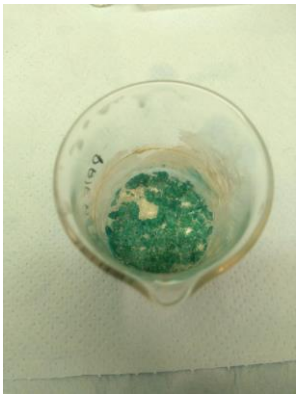

Appendix J – NIPAM NMR.

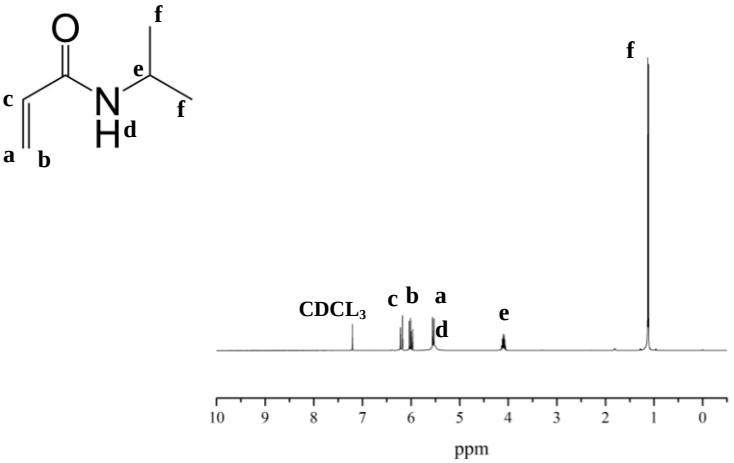

Appendix K – Colour transformation after hours due to oxidation of the activator (Conversion of $Cu^{I}Br$ to $Cu^{II}Br_2$).